Relationship between hygroscopicity and cloud condensation nuclei activity for urban aerosols in Tokyo

Michihiro Mochida[1*], Mikinori Kuwata[2], Takuma Miyakawa[2], Nobuyuki Takegawa[2], Kimitaka Kawamura[1] and Yutaka Kondo[2]

[1] Institute of Low Temperature Science, Hokkaido University,
N17, W8, Kita-ku, Sapporo 060-0819, Japan

[2] Research Center for Advanced Science and Technology, The University of Tokyo,
4-6-1 Komaba, Meguro-ku, Tokyo 153-8904, Japan

*Corresponding author (e-mail: mochida@pop.lowtem.hokudai.ac.jp)

Submitted to Journal of Geophysical Research - Atmospheres

Abstract:

As described by the Köhler theory, the hygroscopicity of atmospheric aerosol particles is a key factor regulating their cloud condensation nuclei (CCN) activity. In this study, the relationship between hygroscopicity and CCN activity for urban aerosol particles was investigated using a hygroscopicity tandem differential mobility analyzer (HTDMA) coupled in series to a CCN counter. The HTDMA-CCNC system was operated near the center of the Tokyo metropolitan area from November 10 to 17, 2004. For aerosol particles whose dry mobility diameters were 30-200 nm, the ratios of CCN to condensation nuclei (CN) at 0.22 -1.3% supersaturation were obtained as a function of particle hygroscopicity at 83 and 89% RH. More-hygroscopic particles were clearly more CCN active than less-hygroscopic particles of the same size, indicating that hygroscopicity is a critical factor regulating CCN activity. The chemical compositions of particles were measured using an aerosol mass spectrometer, and were found to relate closely to CCN activity as well as to the hygroscopicity. The measured CCN–hygroscopicity relationships were compared to those predicted by Köhler theory. The results suggest that CCN activity is possibly perturbed by changes in surface tension due to organics, dissolution/dissociation of water-soluble organics under supersaturation conditions, or different non-ideality of organics from inorganic salts. These factors associated with organics are potentially important for CCN numbers and thus for cloud processes in the atmosphere.

1. Introduction

The effect on climate of anthropogenic sources is one of the major concerns in current global environmental issues. In particular, indirect forcing of atmospheric aerosols via the formation of cloud droplets is an important scientific problem because it currently leads to large uncertainty in the prediction of the radiative forcing and of its perturbation by human activity. Chemical compositions of aerosol particles released from natural and anthropogenic sources are not homogeneous either locally or globally, hence characteristics such as hygroscopicity and surface tension are significantly different from one particle to another, controlling the particle's ability to form cloud droplets. In particular, organic components in particles contribute significantly to CCN concentrations under various conditions [*Novakov and Penner*, 1993; *Matsumoto et al*., 1997], and their complex characteristics make the prediction of cloud droplet formation a challenging research subject.

Recently, a number of model studies dealing with the role of organics in cloud formation have been presented [e.g., *Chuang et al*., 1997; *Feingold and Chuang*, 2002; *Nenes et al*., 2002; *O'Dowd et al.*, 2004; *Lance et al*., 2004; *Abdul-Razzak and Ghan*, 2004]. Theoretically, cloud droplet formation is enhanced by the dissolution of water-soluble organics and the reduction in surface tension by surface-active materials. By contrast, organic films may deplete droplet formation by retarding the transfer of water from gas phase to particles [*Feingold and Chuang*., 2002]. A sensitivity study for the prediction of cloud droplet numbers dealing with the above factors suggests that uncertainty in the chemical compositions of aerosol particles strongly contributes to the variability of cloud droplet numbers [*Lance et al*., 2004]. The importance of reduction of surface tension is in particular discussed in several studies [*Nenes et al*., 2002; *Lance et al*., 2004]. However, attempts to measure the surface tension of real particles in the atmosphere are limited [*Facchini et al.*, 1999; 2000], and insufficient to estimate the surface tension of atmospheric aerosol particles

under various conditions. Further, a lack of information on the bulk hygroscopicity (i.e., solute effect) of organics also limits our prediction of cloud droplet formation. Only one constant value of hygroscopicity has been applied in global models dealing with direct and/or indirect effects of organic aerosols [*Ghan et al.,* 2001a, 2001b] despite the fact that the hygroscopicity of organics is recognized to vary depending on their sources and ages [*Saxena et al*., 1995]. Moreover, the role of the partial dissolution of organics in cloud condensation nuclei (CCN) activity is still under debate. Perturbation of CCN activity due to the partial dissolution of organics has been evaluated by model studies [e.g., *Schulman et al*., 1996], whereas laboratory experiments imply that particles of slightly water-soluble organics can act as effective CCN as if they were completely soluble [*Raymond and Pandis*, 2003].

All of the issues described above stimulate the investigation of CCN activity from the viewpoint of particle characteristics other than size. For instance, field measurements using a hygroscopicity tandem differential analyzer (HTMDA) draw attention as a means of measuring the hygroscopicity of particles, a key property for CCN activity [*Köhler*, 1936]. A number of hygroscopicity studies have been conducted in urban and remote sites, inferring its relevance to CCN activity. In some field studies, hygroscopicity and CCN activity have been measured simultaneously for mono- and poly-dispersed aerosol particles using a HTDMA and a CCN counter in parallel [*Brechtel and Kreidenweis*, 2000a; *Zhou et al.*, 2001; *Roberts et al*., 2002; *Dusek et al.* 2003; *Rissler et al.*, 2004]. These studies have suggested that hygroscopicity is a factor regulating the CCN activity of particles.

In this study, the relationship between hygroscopicity and CCN activity for urban aerosol particles over Tokyo was investigated using a novel instrumental setup: a HTDMA coupled in series to a CCN counter. The HTDMA was used to classify particles according to their hygroscopicity under subsaturation RH conditions (83 and 89 %), and the CCN counter measured the number of CCN particles at supersaturation RH (0.22 to 1.3 %) among the

91 particles classified by their hygroscopicity. This HTDMA-CCNC system enabled us to
92 measure the CCN activity of urban aerosol particles as functions of dry particle size and of
93 their hygroscopicity. As far as we know, this is the first report in which CCN activities have
94 been investigated for atmospheric particles with specific sizes and hygroscopicities. Here we
95 present results from simultaneous measurements of hygroscopicity and CCN activity of
96 atmospheric particles, and discuss new insights concerning the behavior of CCN and thus
97 mechanisms for the formation and growth of cloud droplets.
98
99 **2. Experimental**
100 **2.1 Köhler theory of the relationship between hygroscopicity and CCN activity**
101 The theory of CCN activation of atmospheric aerosol particles was presented by
102 *Köhler* [1936], where the activation was explained by the thermodynamic balance of two
103 effects: a decrease in water vapor pressure due to the solute (Raoult effect) and an increase in
104 water vapor pressure due to the curvature at the air-liquid interface (Kelvin effect). For
105 single-solute particles, the equilibrium water vapor saturation ratio S for a droplet can be
106 described by:
107
108 $$\ln S = \frac{2A}{d_{\mathrm{wet}}} - \frac{B d_{\mathrm{ve,dry}}^{\ 3}}{d_{\mathrm{wet}}^{\ 3} - d_{\mathrm{ve,dry}}^{\ 3}} \qquad \left(A \equiv \frac{2\sigma M_w}{\rho_w RT},\ \ B \equiv \nu\phi \frac{M_w \rho_s}{M_s \rho_w} \right) \tag{1}$$

109
110 where d_{wet} and $d_{\mathrm{ve,dry}}$ are the diameter of the droplet and the volume equivalent diameter of the
111 dry (solute) particle, respectively, σ is the surface tension, M_{w} and M_{s} are the molecular
112 weights of water and solute, respectively, ρ_{w} and ρ_{s} are the density of the water and solute,
113 respectively, ν is the degree of dissociation, and ϕ is the osmotic coefficient. The product of ν
114 and ϕ is equivalent to the so-called van't Hoff factor [*Pruppacher and and Klett*, 1997]. R and

115 T are the gas constant and temperature, respectively. This equation can be extended for a
116 multi-component system, by modifying the hygroscopicity B in Equation 1 to be
117
118 $$B = \frac{M_w}{\rho_w} \sum_i \frac{\nu_i \phi_i \varepsilon_i m_i}{M_i} \Bigg/ \sum_i \frac{m_i}{\rho_i} \quad (2),$$
119
120 where ν_i, ϕ_i, ε_i, m_i, M_i are the degree of dissociation, the osmotic coefficient, the degree of
121 dissolution, the mass mixing ratio, and the molecular weight of compound i, respectively. This
122 equation is based on the additive effect of solutes, including inorganics and organics.
123 Insoluble compounds such as elemental carbon, crustal materials and hydrophobic organics
124 may also be included in Equation 2, by regarding M_i to be infinity. Note that, as expressed
125 above, the term hygroscopicity in this paper denotes bulk hygroscopicity, and does not include
126 the Kelvin effect of aerosol particles.
127 Assuming that A and B are constants and that d_{wet} is much larger than $d_{\mathrm{ve,dry}}$, we can
128 obtain the critical water vapor saturation ratio S_{c}, i.e. the minimum saturation ratio S required
129 to form cloud droplets, with A, B and $d_{\mathrm{ve,dry}}$ from
130
131 $$\ln S_{\mathrm{c}} = \frac{2}{\sqrt{B}} \left(\frac{2A}{3 d_{\mathrm{ve,dry}}} \right)^{3/2} \cong s_{\mathrm{c}} \quad (3),$$
132
133 where s_{c} is the critical water vapor supersaturation ($S_{\mathrm{c}} = 1 + s_{\mathrm{c}}$). CCN activity of the particles
134 is therefore high when the hygroscopicity B and dry diameter $d_{\mathrm{ve,dry}}$ are large, and when the
135 surface tension σ is low (i.e. A is low). This study aims to determine simultaneously the
136 hygroscopicity and CCN activity of atmospheric aerosol particles, and to assess the
137 relationship based on Equations 1-3.

138

139 **2.2 Atmospheric Measurement using HTDMA-CCNC System**

140 The experimental setup of the HTDMA-CCNC system is presented in Figure 1. In the
141 HTDMA part, sample atmospheric aerosols (PM1) were dried in tandem diffusion dryers (TSI
142 Model 3062) filled with silica gel and molecular sieve (13X/4A, Spelco). The reading of a RH
143 sensor (Vaisala HMP237, uncertainty: 2% RH, calibrated at 11.3 and 75.3% RH with LiCl and
144 NaCl saturated solutions) at the outlet of the dryers was below 2% during the HTDMA
145 operation. The RH of the dried aerosols was thereby estimated to be < 4% (= 2% + the
146 uncertainty of the sensor). The sample aerosols were then neutralized in an ^{241}Am bipolar
147 charger, and classified using a differential mobility analyzer (DMA1, TSI Model 3081). The
148 RH of the sample aerosols was then controlled by a supply of water vapor through a Nafion
149 tube, and the resulting size change of aerosol particles was measured by another DMA
150 (DMA2) combined to a condensation nuclei (CN) counter (TSI Model 3022A). The RH of the
151 circulated sheath flow of DMA2 was also controlled by water vapor exchange through a
152 Nafion tube. The residence time of particles between the outlet of the Nafion humidifier and
153 the inlet of DMA2, which allows particles to equilibrate with the humidified air, was about 10
154 s. Details of the HTDMA used in this study have been given elsewhere [*Mochida and*
155 *Kawamura*, 2004]. Being different from the work in *Mochida and Kawamura*. [2004], fixed
156 RH conditions in DMA2 were achieved as follows. The RH of both the sample and sheath
157 flows entering DMA2 were controlled by changing the mixing ratios of the humidified and
158 dry air flows supplied as sheath flows to the Nafion tubes. The mixing ratio was adjusted
159 automatically by a Proportional-Integral-Derivative (PID) control with the RH as the input.
160 The RH in DMA2 is defined as the weighted average of RH in the sheath and sample airs by
161 their flow rates. The temperature of the sheath (sample) air was 297.6 ± 0.7 (297.8 ± 0.7) K.
162 An extra Nafion dryer was placed at the outlet of DMA2, so that a dehumidified aerosol

(~10% RH) was introduced to CN and CCN counters and a volatility TDMA (VTDMA) system (see Figure 1).

Part of the processed sample aerosol exiting DMA2 was introduced to the CCN counter [*Roberts and Nenes*, 2005] (Droplet Measurement Technologies, Boulder, CO) at a sample flow rate of 0.05 liter min^{-1}. This CCN counter can establish supersaturation conditions between 0.1 to 2% in a cylindrical continuous-flow thermal-gradient diffusion chamber. The total flow rate in the chamber was 0.5 liter min^{-1} and the residence time of aerosol particles in Poiseuille flow was ca. 13 s. The CCN number concentration was measured as a function of the resulting size distribution (i.e. the hygroscopic growth factor g, or hygroscopicity B). The sheath flow rate of the CCN counter was 0.45 liter min^{-1}. The particle free sheath flow was generated from room air by letting the air pass through a HEPA filter. According to Boltzmann equilibrium of particle charging and the transfer function of the DMA columns, the number of aerosol particles decreases by processing through two DMAs in series. However, the resulting number concentrations of particles (typically 1-20 particles cm^{-3}) were well above the detection limit of the CN and CCN counters with integration times of 3 min. The diameters of initially dry particles ranged from 30 to 200 nm in the experiments. The RH after humidification was set to be 83 and 89 %, depending on the sampling period. Unless otherwise stated, diameter in this paper means an electrical mobility diameter (d_{mob}) classified by a DMA. Note that the mobility diameter of classified particles has a finite size range (geometric standard deviation: 1.04 for 100 nm particles). Further, small but non-negligible fractions of particles have larger diameters (~ ×1.5 or more) because of multiple electrostatic charges.

An Aerosol Mass Spectrometer (AMS, Aerodyne) was operated in parallel to the HTDMA-CCNC system to obtain the chemical compositions of aerosol particles. Details of the AMS measurements are described in *Jayne et al.* [2000] and *Takegawa et al.* [2005]. Mass

188 concentrations of chemical components integrated over specific ranges of vacuum
189 aerodynamic diameter (d_{va}) measured by the AMS were used to represent the chemical
190 compositions of mono-disperse aerosol particles in the HTMDA-CCNC system. Since the
191 ratio of d_{va} to electrical mobility diameter (d_{mob}) can vary depending on particle morphology
192 and density [*DeCarlo et al.*, 2004], we present here the mass concentrations at d_{va} ranging
193 from 50 to 200 nm as estimates of the compositions at d_{mob} = 100 nm. The chemical
194 compositions of particles with other mobility diameters used in the HTDMA-CCNC study
195 were not estimated, but the general characteristics may be qualitatively similar to that at d_{mob}
196 = 100 nm.

197 As shown in Figure 1, the VTMDA system with a 400 °C heater was connected to the
198 HTDMA in parallel to the CN and CCN counters. This part of the measurement system was
199 used to quantify the amount of non-volatile components (mainly elemental carbon) in the
200 particles. The results from the instrument are presented in a separate paper [*Kuwata et al*.,
201 2006].

202 In parallel to the HTDMA-CCNC and the AMS, a Scanning Mobility Particle Sizer
203 (SMPS, TSI Model 3034) was operated separately to measure the size distribution of ambient
204 particles. Two diffusion dryers with silica gel in series (TSI Model 3062) were placed in front
205 of the SMPS. The mobility size distributions of dry particles were obtained every 3 min.

206 The aerosol measurements using the HTDMA-CCNC system were carried out at the
207 Research Center for Advanced Science and Technology, the University of Tokyo, Tokyo,
208 Japan from November 10 to 17, 2004. The population of the Tokyo metropolitan area is 41
209 million, and the measurement site is located near the center of the area. Several different types
210 of measurements were performed during the campaign. From November 10 to 12, temporal
211 variation of hygroscopicity and CCN activity of aerosol particles were obtained
212 semi-continuously for particles whose dry diameters were 100 nm. From November 12 to 16,

213 particles whose dry diameters were 30, 50, 80, 100, 150, and 200 nm were measured
214 periodically. During the period of November 10-16, the hygroscopicities of particles were
215 measured at 83% RH. On November 17, the hygroscopicities for 50 and 100 nm particles
216 were measured at 89% RH. Only a limited number of samples were measured at 89% RH
217 because of the limited period of the investigation.

218 Particle number distributions as a function of hygroscopicity was measured every hour
219 during the field measurements, with a scanning time of 5 min. In the 55-min interval, we
220 measured CCN activities every 5 min by changing the particle diameters of the humidified
221 particles (hygroscopicity), and supersaturation RH. Four different supersaturation conditions,
222 0.22, 0.55, 0.82 and 1.3% (determined by Köhler- and Pitzer equations, see explanations in
223 section 2.4), were applied to the CCN activity measurements. Dry particle diameters were
224 also changed periodically, usually after the 1-hour measurement cycle described above.

225

226 **2.3 Calculation of Hygroscopicity from Hygroscopic Growth Factor**

227 The hygroscopic growth factor g, which can be measured using the HTDMA, is the
228 ratio of the humidified to dry particle diameters:

229

230 $$g = \frac{d_{\mathrm{ve}}(RH)}{d_{\mathrm{ve,dry}}} \cong \frac{d_{\mathrm{mob}}(RH)}{d_{\mathrm{mob,dry}}} \quad (4)$$

231

232 where $d_{\mathrm{ve,dry}}$ and d_{ve}(RH) (or $d_{\mathrm{mob,dry}}$ and d_{mob}(RH)) are the dry and humidified
233 volume-equivalent (or mobility) diameters of particles in the HTDMA, respectively. This
234 hygroscopic growth factor g is a function of RH, which increases with increasing RH. In this
235 study, $d_{\mathrm{mob,dry}}$ is approximated by the mobility diameter of particles under the condition of
236 <4% RH in DMA1. The second term on the right side of Equation 1 is expressed with water
237 activity a_{w} by

$$\ln a_w = -\frac{Bd_{\mathrm{ve,dry}}^{\ 3}}{d_{\mathrm{ve}}(RH)^3 - d_{\mathrm{ve,dry}}^{\ 3}} \cong -\frac{Bd_{\mathrm{mob,dry}}^{\ 3}}{d_{\mathrm{mob}}(RH)^3 - d_{\mathrm{mob,dry}}^{\ 3}} \quad (5)$$

under sub-saturated conditions. Equations 1, 4 and 5 give the relationship between the bulk hygroscopicity B and the hygroscopic growth factor g:

$$B = \left(1 - g^3\right)\ln a_w \quad (6).$$

Under sub-saturated RH conditions in the HTDMA, a_w is nearly equal to the saturation ratio S (or $RH(\%)/100$) in equilibrium conditions, but slightly different from S, due to the surface tension effect (Kelvin effect) of particles. The relationship between S and a_w is given from Equations 1 and 5 by:

$$S(\equiv RH(\%)/100) = a_w \exp\left(\frac{2A}{d_{ve}(RH)}\right) \quad (7).$$

From Equations 6 and 7, both a_w and B can be calculated from RH and g that are directly measured by the HTDMA, and from the surface tension σ that is assumed appropriately. Since the prediction of a_w is less sensitive to the uncertainty in σ than that in RH, application of the surface tension of pure water is a reasonable assumption for the prediction of B. An important point is that hygroscopicity B in Equation 6 is the value derived under subsaturation RH conditions, which is not necessarily the same as that in Equations 1-3 under supersaturated conditions. This is because ν, ϕ, and ε are not necessarily constant. For instance, in the case of $(NH_4)_2SO_4$ and NH_4NO_3 particles whose dry diameters are 100 nm,

261 the hygroscopicity B at 83% RH, 298 K are calculated to be 0.79 and 0.66 times, respectively,
262 smaller than those at the critical supersaturation, 308 K. This is the point to be discussed in
263 the results and discussion section.
264
265 **2.4 Derivation of the CCN distribution as a function of hygroscopicity**
266 Particle number (CN) distributions as a function of hygroscopic growth factor were
267 obtained by scanning DMA2 and by recording the number of particles exiting from DMA2,
268 with a size resolution of 64 channels/digit. An example of the scan is shown as a white
269 histogram in Figure 2a. Based on this CN distribution as a function of g, the distribution of
270 CCN was obtained as follows. CCN numbers were measured at four different hygroscopic
271 growth factors g, 1.00, 1.11, 1.24, and 1.38 (shown as solid circles in Figure 2a). The
272 distributions of hygroscopic growth factors of particles entering the CCN counter for four
273 different set points, $k_j(g)$ (j = 1,2,3 and 4), were estimated from the experimentally derived
274 transfer function of the first and second DMAs (Figure 2b); the mono-disperse size
275 distribution of $(NH_4)_2SO_4$ particles processed in the HTDMA under dry conditions ($d_{mob,dry}$ =
276 30-200 nm) was measured by using DMA2 and the CN counter as SMPS, and was
277 approximated to be the transfer functions for the atmospheric particles with the same $d_{mob,dry}$.
278 A fixed half-width of the distribution was applied for particles with different g. Although the
279 transfer functions of DMA2 for particles that grow by humidification are different from those
280 for dry particles (Cunningham slip correction is not constant), the error of the half-width
281 associated with this simplification was estimated to be at most 4%. As seen in Figure 2b,
282 particles with some width of hygroscopic growth factor are introduced to the CCN counter
283 even if the classification in the HTDMA is fixed. Figure 2b further shows that the
284 combination of each distribution well covers the entire range of the measured hygroscopic
285 growth factor g. Weighting functions w_j (g) (j = 1,2,3 and 4) presented in Figure 2c are

derived from $k_j(g)$ by the equation:

$$w_j(g) = k_j(g) \Big/ \sum_j k_j(g) \quad (10),$$

and are presented in Figure 2c. The CCN distributions as a function of hygroscopicity are then calculated based on the equation:

$$\frac{dy_{CCN}(g)}{d\log g} = \frac{dy_{CN}(g)}{d\log g} \sum_{j=1}^{4} w_j(g) r_j \quad (11)$$

where r_j is the CCN/CN ratio at four set points of hygroscopic growth factors g, and $y_{CN}(g)/d\log g$ and $y_{CCN}(g)/d\log g$ are number concentrations of CN and CCN as a function of g, respectively. An example of the calculated CCN distribution as a function of g is presented as the shaded histogram in Figure 2a.

2.5 Uncertainty in the Measurements

There are three different types of uncertainties in the variables used in this study; i.e. random errors (precision), systematic errors (trueness), and widths of diameter and supersaturation with respect to the mean values. They are summarized in Table 1. Random errors and widths of variables in this paper are presented as one standard deviation (1SD). In this study, any fluctuations in variables under fixed conditions were considered as random errors, even though their frequencies were longer than the sampling rates of the variables. Random and systematic errors are discussed and presented separately in this paper, which makes it possible to assess whether small differences in hygroscopicity and CCN activity are statistically significant.

310 The random errors in CN and CCN counts were statistically determined to be 1-4%
311 and 2-10%, respectively (Table 1). The random error in the CCN to CN ratio is 2-11%. The
312 systematic error in the CCN/CN ratio was estimated to be less than 10%.
313 The classification of the first and second DMAs is calibrated by measuring the sizes of
314 standard PSL spheres (STADEX, 70±1 nm, CV 6.22%; 123±2 nm, CV 1.54%; 207±6 nm, CV
315 1.62%) in the SMPS mode. The size selection of two DMAs was further adjusted by
316 classifying dry $(NH_4)_2SO_4$ particles with one DMA and by measuring the mode diameter with
317 the other. The same procedure was performed between the second DMA and another (third)
318 DMA used for the calibration of the CCN counter (see section 2.2). Mobility diameters based
319 on the PSL calibration of DMA2 are presented in this paper. Precisions of the mobility
320 diameters of particles classified in the first and second DMAs were 1%. The width of d_{mob}
321 classified by the DMAs was estimated to be 4% from size distribution measurements of PSL
322 spheres. Errors associated with the assumption of particle morphology (i.e., $d_{ve} = d_{mob}$) are
323 discussed in the results and discussion section (section 3.4.3).
324 Supersaturation in the CCN counter was calibrated by measuring the critical activation
325 dry diameters of $(NH_4)_2SO_4$ particles classified using a DMA. In the calibration procedure,
326 the CCN/CN ratio measured for $(NH_4)_2SO_4$ particles is ideally a stepwise function of the dry
327 particle diameters, but it actually shows a gradual increase as a function of the dry diameter.
328 This is due to the width of the supersaturation condition inside the CCN counter, and also of
329 the particle size classified by the DMA. If the widths of critical diameters are assumed to be
330 totally from those of supersaturation in the CCN counter, we can obtain the widths of
331 supersaturation to be ±0.02, ±0.03, ±0.06 and ±0.08% for 0.22, 0.55, 0.82 and 1.3 %,
332 respectively. In this paper, we present supersaturation conditions based on the calibration
333 using the $(NH_4)_2SO_4$ on the assumption of Köhler curves at $T = 308$ K, with ϕ calculated from
334 the Pitzer equation [*Pitzer and Mayorga*, 1973] (hereafter referred to as KP). The droplet

surface tension of $(NH_4)_2SO_4$ in this calculation is based on the relationship in *Hänel* [1976].

As presented in *Kreidenweis et al.* [2005], some available CCN activation models predict a significantly higher critical supersaturation of $(NH_4)_2SO_4$ than that from KP. In the discussion section, we also apply the empirical model proposed by *Kreidenweis et al.* [2005] (hereafter referred to as K2005) to assess the potential uncertainty of the supersaturation conditions. This model is chosen for comparison because its prediction of critical supersaturation is highest among the models summarized in *Kreidenweis et al.* [2005]. Because K2005 is based on a parameterization at 298 K, a correction factor of 0.952 $\{=(298/308)^{3/2}\}$ derived from Equations 1 and 3 was applied to determine s_c at 308 K. Note that the standard Köhler model with $\phi = 1$, by contrast, gives a lower critical supersaturation than KP with the Pitzer equation. However, the discrepancy is smaller than that between KP and K2005.

The systematic error of RH measurement in the HTDMA is ≤ 2% above 83 % RH, based on the manufacturer's warrant of the RH sensors (Vaisala, HMP 237). The random errors of RH at the inlet and outlet of DMA2 were determined to be 0.3% and 0.9%, respectively, from the temporal variations of the RH readings. Possible drift of the sensitivity of the RH sensors was assessed by a 4-day continuous measurement of hygroscopic growth factor g for 100 nm $(NH_4)_2SO_4$ particles at 83% RH, which was performed after the field measurement. The 1SD value of g for $(NH_4)_2SO_4$ was 0.01 (n = 1100), which is explained by 0.5% error in RH. This RH error is in the range of the precisions of the RH reading (0.3-0.9%). The possible drift of RH associated with the sensitivity change of the RH sensors is thereby neglected in this study. The systematic error of RH (≤ 2%) leads to ≤ 2% error in hygroscopic growth factor g, for particles whose hygroscopic growth factor is about 1.2 at 80-85% RH [*Mochida and Kawamura*, 2004].

The hygroscopic growth factor g of pure $(NH_4)_2SO_4$ particles at 83% RH in DMA2

were measured (n = 2) during the field investigation. They measured g were within 2% of that predicted in the literature [*Tang and Munkelwitz*, 1994], which also supports the validity of the RH control in HTDMA. The random error of g is determined to be 1% from the growth factor measurements of 100 nm $(NH_4)_2SO_4$ particles at 83% RH after the field investigation.

As described in section 2.3, whether or not the hygroscopicity of particles under supersaturation conditions at 308 K (B_{SS}) reflects those at 83% and 89% RH, 298 K (B_{83} and B_{89}) is important for the discussion. If major inorganic salts in sample atmospheric aerosols remain as solids after they are humidified in the HTDMA, then this leads to a large difference between B_{83} (or B_{89}) and B_{SS} by change of ε in Equation 2. However, we conclude that this is very unlikely under our experimental conditions, based on the following results. First, when pure $(NH_4)_2SO_4$ particles of 30-200nm were introduced to the HTDMA system at the RH set points of 83 and 89%, the particle growth expected from its deliquescence was always observed for all particle size ranges, indicating that $(NH_4)_2SO_4$ does deliquesce under our experimental conditions. This result is consistent with another HTDMA study [*Hämeri et al*., 2000]. Second, since other possible major components of inorganic salts, such as NH_4NO_3, NH_4Cl, H_2SO_4, NH_4HSO_4, $(NH_4)_3H(SO_4)_2$ have lower bulk deliquescence RH than $(NH_4)_2SO_4$, these fractions in atmospheric particles should also deliquesce in the HTDMA system. Third, these inorganic salts are mixed with organics in the atmosphere, and laboratory and field studies show evidence that they usually deliquesce at lower RH than pure salts [*Dick et al.*, 2000; *Xu et al*., 2003].

Other factors that potentially alter B as a function of RH are discussed in the results and discussion section. They include a change in osmotic coefficient ϕ of inorganic salts, and changes in $\nu\phi$, and ε of organic compounds.

Note that, although the uncertainty in the measurements was quantified as much as possible, there are several potential biases that have not been fully quantified in this study.

They include possible changes in the particle chemical composition and morphology in the apparatus. When atmospheric particles were introduced to the HTMDA under dry (<4% RH) conditions in DMA2, no significant decrease in d_{mob} was observed. This implies that, at least between DMA1 and DMA2, evaporation/condensation of semi-volatile compounds and the particle morphology change is negligible under the dry condition. However, possible changes in the composition and morphology in other parts of the apparatus and in different RH conditions were not assessed in this study. Possible evaporation of components in the CCNC at increased temperatures (up to 308 K) and possible absorption of water-soluble gases by the growing droplets were not assessed either.

Another possible bias is that organics in particles retard water uptake by particles [*Feingold and Chuang*, 2002], which prevents particles in the CCNC column reaching the critical droplet diameter in the residence time of < 13 s. The same mechanism is probably not important in the HTMDA part because the kinetic study of hygroscopic growth of urban aerosol particles in Mexico City shows that the fraction of particles whose time scale of hygroscopic growth is longer than 2-3 s is only <2% for 50 and 100 nm particles [*Chuang*, 2003].

3. Results and Discussion

3.1 General characteristic of the atmospheric aerosol conditions

The primary objective of this study is to assess the relationship between the hygroscopicity and CCN activity of atmospheric particles, based on HTDMA-CCNC measurements for urban aerosols over Tokyo. The general characteristics of the hygroscopicity and CCN activity, as well as the chemical compositions of aerosol particles during the investigation is briefly presented in this section.

410 **3.1.1 Chemical compositions**

411 Table 2 summarizes the means and ranges of the relative abundances of major
412 chemical species that were obtained by the AMS for particles whose d_{va} ranged from 50 to
413 200 nm. As presented in Table 2, organics is the dominant compound class (mean: 54 %).
414 Such high abundances of organics were also observed in previous AMS studies in Tokyo
415 [*Takegawa et al*., 2006], and are interpreted as a result of the large contribution of motor
416 vehicle emissions. The AMS spectra indicate the presence of both hydrocarbon-like and
417 oxygenated organics (see section 3.6); the former is mainly primary in origin whereas the
418 latter is secondary [*Zhang et al.*, 2005a]. The sums of water-soluble inorganic ions (NO_3^-,
419 SO_4^{2-}, Cl^- and NH_4^+) are 23% on average. The ratio of organics to water soluble inorganic
420 ions is on average 2.8. The dominance of organic components suggests their important effect
421 on the CCN activity of urban aerosol particles.

422

423 **3.1.2 Hygroscopic growth factor**

424 Figure 3 presents the averaged distribution of hygroscopic growth factor during the
425 investigation, for particles whose dry diameters were 100 nm. Hygroscopicity *B* was also
426 calculated as a function of humidified particle diameters and is presented at the top of Figure
427 3. As shown in Figure 3, particle growth of mono-dispersed particles ($d_{mob,dry}$ = 100 nm) by
428 the addition of water vapor leads to a bimodal distribution. This indicates that aerosol
429 particles are externally mixed, i.e., chemical compositions are different from particle to
430 particle. The bimodal distribution is similar to those reported for the urban atmosphere
431 [*Heintzenberg, et al*., 1998, *Gasparini et al*., 2004]. The deviation of the distribution
432 presented as the hatched area suggests that the relative abundance of particles in more and less
433 hygroscopic modes, and also those in between, varied substantially depending on the time
434 period during the investigation.

435 The mode diameter of less-hygroscopic particles after humidification was nearly equal
436 to the dry diameter. The VTDMA shows that less-hygroscopic particles were less volatile,
437 which suggests that the less hygroscopic particles were mainly composed of elemental carbon.
438 The mode of hygroscopicity of more hygroscopic particles (B ~0.2-0.4) was substantially
439 lower than the hygroscopicity of pure $(NH_4)_2SO_4$ and NH_4NO_3 (B = 0.5 for both compounds).
440 Further, the number fraction of particles whose hygroscopicities corresponded to that of pure
441 $(NH_4)_2SO_4$ and NH_4NO_3 were negligibly small. Based on this result as well as the chemical
442 composition of particles (Table 2), it is concluded that the more-hygroscopic particles are
443 composed of an internal mixture of organics and inorganic salts such as ammonium sulfates
444 and nitrates.
445
446 **3.1.3 CCN size distribution**
447 Figure 4 presents examples of CN and CCN size distributions averaged from
448 November 14 to 15 at supersaturation of 0.22, 0.55, 0.82 and 1.3%. As shown in Figure 4, the
449 range of dry diameters classified by DMA1 in this study (30-200 nm) cover the dominant
450 particle size ranges of CCN during this study. While the CCN/CN ratio starts to decrease
451 toward the smaller particle diameters below $d_{mob,dry}$ = 200 nm, the mode diameters of the CCN
452 number distributions were smaller, at around 100-150 nm. This is because the CN distribution
453 has a maximum in the 30-100 nm range. This suggests that the decreasing trend of the
454 CCN/CN ratio toward smaller particle diameter is compensated for by the increasing trend in
455 particle numbers. The total CCN number (integrated area in Figure 4) is thereby sensitive to
456 changes in critical dry diameters for the CCN, suggesting the importance of chemical
457 compositions that control the critical activation dry diameters by regulating hygroscopicity B
458 and surface tension σ (and A) in Equation 3.
459

460 **3.2 CCN/CN ratios for particles with different hygroscopicity**

461 Using the HTDMA-CCNC system, the CCN/CN ratios were obtained for four
462 different hygroscopic growth factors (or hygroscopicities) of ambient particles. Figure 5
463 summarizes all the data of the CCN/CN ratios collected during the sampling period. The
464 ratios were measured under the conditions of (1) hygroscopic growth factors of 1.00, 1.11,
465 1.24 and 1.38, (2) dry particle diameters of 30, 50, 80, 100, 150 and 200 nm, and (3) RH in
466 the HTDMA of 83 and 89%. Figure 5 clearly shows that the CCN/CN ratios strongly depend
467 on the conditions of supersaturation, hygroscopicity, and dry particle diameters. For instance,
468 for 30 nm particles under the RH condition of 83% in the HTDMA (Figure 5a), significant
469 numbers of CCN were observed only at the highest supersaturation of 1.3%, and
470 hygroscopicity above 1.24. In the case of 50 nm particles (Figure 5b), the spectra of CCN/CN
471 ratios versus hygroscopicity are clearly different from those of 30 nm particles; more CCN
472 was observed for each hygroscopicity and supersaturation than in the case of 30 nm particles.
473 For the particle diameters ≥80 nm, the CCN/CN ratios with hygroscopic growth factor g
474 ≥1.11 were almost unity except for the case of supersaturation at 0.22%. For particles whose
475 dry diameters were 150 and 200 nm, the CCN/CN ratios with $g \geq 1.11$ were observed to be
476 unity under all supersaturation conditions (0.22-1.3%).

477 In general, larger particles are more CCN active than smaller particles (Figures 5a-e).
478 This is consistent with Köhler theory; the more the amount of solute, the larger the resulting
479 droplet diameter (Raoult effect) becomes, being in favor of the CCN activation in terms of the
480 surface tension (Kelvin) effect. Furthermore, it is also evident that particles with higher
481 hygroscopic growth factor g are more CCN active than those with lower g. The higher growth
482 factor means higher hygroscopicity B, leading to lower critical supersaturation as written in
483 Equation 3.

484 Limited numbers of data were also collected under the condition of 89% RH in the

HTDMA (Figures 5g and h). The results indicate that the spectra of the CCN/CN ratios versus hygroscopic growth factor for various supersaturations obtained for 50 and 100 nm particles were generally lower than those obtained at 83% RH (Figures 5b and 5d). Although the CCN/CN ratios should not always be the same at different time periods, this trend can be explained by the theory that particles with some hygroscopicity *B* show larger hygroscopic growth factor *g* at higher RH in the HTDMA.

3.3 Time series of the CCN distribution as a function of hygroscopicity

Based on the method described in the experimental section, semi-continuous distributions of CCN numbers as a function of hygroscopic growth factor *g* were calculated. Figures 6a-c present temporal variations of the CN and CCN distributions as a function of *g* for 100 nm particles on November 10-12. The z-axis unit is d*N* (particle cm^{-3})/dlog *g*, and the particle numbers integrated along the y-axis are equal to those at the inlet of DMA2. Since the transfer function of DMA1 does not change with time, the integrated number is proportional to the number of 100 nm particles in the atmosphere. Chemical compositions of aerosol particles obtained by the AMS (50 nm < d_{va} < 200 nm) are also presented in Figure 6d, as estimates of the compositions of particles at $d_{mob,dry}$ = 100 nm.

Figure 6a shows the number distribution of aerosol particles (CN) as a function of hygroscopic growth factor *g*. As was presented in Figure 3, bimodal distributions were observed, one for less-hygroscopic and the other for more-hygroscopic particles. The increase in the number concentrations of both particles in the time periods 22:00, November 10 to 12:00, November 11 and 3:00-19:00, November 12 is in accordance with the aerosol mass change detected by the AMS (Figure 6d), supporting the validity of the HTDMA measurements. A sharp increase in the numbers of more-hygroscopic particles ($g \sim 1.4$) at around noon on November 11 (Figure 6a) is coincident with the increase in the mass of SO_4^{2-}

and NO_3^- (Figure 6d). The number concentrations of less-hygroscopic particles positively correlate with that of the estimated elemental carbon in Figure 6d. This is consistent with the result that more-hygroscopic particles are composed of non-refractory components, whereas less-hygroscopic particles are mainly composed of non-volatile components [*Kuwata et al.*, 2006]. As explained in section 3.1.2, the hygroscopic growth factor of more-hygroscopic mode particles (g = 1.2-1.4) were substantially lower than those of $(NH_4)_2SO_4$ and NH_4NO_3 (g~1.5), indicating that organics whose hygroscopicity is lower than inorganic salts are major components in more-hygroscopic mode particles. In particular, during the time period from 23:00, November 10 to 7:00, November 11, a fraction of the particles whose hygroscopic growth is intermediate (1.1-1.2) increased, suggesting that the organic fraction became substantial during the time period.

Number distributions of CCN, instead of CN, as a function of hygroscopic growth factor g are novel datasets that were obtained for the first time by our newly developed HTDMA-CCNC system. Figures 6b and 6c present CCN distributions at 0.22% and 0.55% supersaturation, respectively, as a function of hygroscopic growth factor g. In the case of 0.22% supersaturation (Figure 6b), some fraction, but not all of the more-hygroscopic particles are detected as CCN. In contrast, almost no particle was detected as CCN for particles in the less-hygroscopic mode. In the case of 0.55% supersaturation (Figure 6c), the numbers of CCN are greater than those at 0.22% supersaturation. In this case, some particles in the less-hygroscopic mode were detected as CCN as well. As explained in section 3.2 and Figure 5, the observed trends in CCN activity between more- and less-hygroscopic particles are consistent with Köhler theory. Figures 6b and 6c further suggest that variation in particle numbers in the atmosphere (Figures 6a and 6d) is also an important factor regulating CCN numbers. For instance, an increase in particle numbers in the more-hygroscopic mode (e.g., at noon on Nov. 11) leads to the increase in CCN numbers shown in Figures 6b and 6c. By

535 contrast, the increase in less-hygroscopic mode particles, shown as red areas in Figure 6a,
536 does not contribute to an increase in CCN numbers. These results indicate the importance of
537 hygroscopicity for the variation of CCN numbers in the atmosphere.
538 The data shown in Figures 6a-d are also presented in Figures 7a-d by normalizing the
539 particle numbers. In the figures, the relative abundances of CN and CCN between more- and
540 less-hygroscopic particles can be seen more clearly. On the normalized distribution basis, the
541 CN and CCN fraction at around g = 1.4 from 11:00, November 11 to 1:00, November 12 is
542 significant, being consistent with the increase in SO_4^{2-} mass fraction shown in Figure 7d.
543
544 **3.4 CCN activity as a function of particle hygroscopicity**
545 The number distributions of CCN as a function of hygroscopicity are subjected to the
546 model assessment using Equations 1-3, to clarify whether or not the hygroscopicity measured
547 by the HTDMA can explain the CCN activity of particles. The limitation of this assessment is
548 that the prediction of CCN numbers based on Köhler theory strongly depends on the estimate
549 of the supersaturation condition in the CCN counter which, as explained in the experimental
550 section, is basically based on the KP approach (see section 2.5). However results from K2005
551 are also discussed in this section.
552 Among the obtained datasets, we have found that the degree of agreement between the
553 models and the measurements is substantially different from sample to sample. First we
554 present a case in which the CCN spectra as a function of hygroscopicity are well explained by
555 Köhler theory on the assumptions that (1) the surface tension is equal to that of pure water, (2)
556 the hygroscopicity at 83% is same as that at supersaturation RH, and (3) KP is appropriate for
557 the prediction of CCN numbers (section 3.4.1). We also present another case in which the
558 deviation of the measured CCN spectra from that predicted with the above assumptions is
559 relatively large (section 3.4.2). Possible errors associated with particle morphology (section

560 3.4.3) and non-constant surface tension and hygroscopicity under supersaturation conditions
561 (section 3.4.4) are also discussed. Note that no assumption about the chemical composition is
562 necessary for the quantitative discussion in this section, and that it is solely based on the
563 theoretical relationship between hygroscopic growth factor g, hygroscopicity B, and critical
564 supersaturation s_c.
565
566 **3.4.1 Case 1: The base model predicts the CCN activity well**
567 Figures 8a-c present number distributions of both aerosol particles (CN) and CCN as a
568 function of hygroscopic growth factor on November 15, 2004. Particles whose dry diameters
569 were 80, 100 and 150 nm were humidified to 83 % in the HTDMA, and CCN at 0.22%
570 supersaturation is presented here. As presented in Equations 1-3, if the dry particle size,
571 supersaturation RH, and the surface tension are provided, we can calculate the minimum
572 hygroscopicity B required for particles to behave as CCN. Further, Equations 5 and 6 give the
573 hygroscopic growth factor g corresponding to the thresholds of B. In Figures 8a-c, the
574 thresholds of B and g calculated based on the assumptions above are presented as vertical
575 thick lines. The ranges of systematic errors, which are associated with that of RH (≤ 2%), are
576 presented with dotted vertical lines. The thresholds of B (and g) are 0.48 (1.48), 0.24 (1.30),
577 and 0.072 (1.11) for 80, 100 and 150 nm particles, respectively. As written above, three
578 assumptions are made in the calculation. First, the hygroscopicity measured at 83% RH by the
579 HTDMA is assumed to well represent that for the supersaturation condition (i.e., B_{83}/B_{ss}=1). It
580 should be noted that this assumption leads to some systematic bias at least for inorganic salts.
581 If the ϕ-RH relationships of $(NH_4)_2SO_4$ and NH_4NO_3 are taken into account for particles
582 whose dry diameters are 100 nm, the B_{83}/B_{ss} ratios are 0.79 and 0.66, respectively. We
583 nevertheless assume B_{83}/B_{ss} to be unity as a base model. The second assumption is that the
584 surface tension of pure water at the critical supersaturation, corresponds to $A = 1.0 \times 10^{-3}$ μm

585 at 308 K. This is reasonable for most inorganic particles [*Brechtel and Kreidenweis*, 2000b],
586 whereas it is possibly not correct for some organic/inorganic mixtures [*Schulman et al*., 1996,
587 *Facchini et al*., 1999]. The third assumption is the determination of supersaturation in the
588 CCN counter by the KP model.

589 Taking into account the width of supersaturation RH in the CCN counter, we further
590 estimated the non-stepwise change in the CCN/CN ratios around the threshold of *B*. Widths of
591 supersaturation without correction of the size widths of $(NH_4)_2SO_4$ particles are used (i.e.,
592 values without parenthesis in Table 1). The absence of the size-width correction is reasonable
593 because dry particles classified in DMA1 in the HTDMA also have the same standard
594 deviation in particle diameters. The derived CCN numbers as a function of hygroscopic
595 growth factor *g* are shown as blue histograms in Figures 8a-c. The error bars represent
596 random errors in the predicted CCN distribution (see section 3.4.2), which however do not
597 include systematic errors (vertical dotted lines). Nearly all of the particles in the
598 more-hygroscopic mode are predicted by the blue histograms. There are some unpredicted
599 CCN at around $g = 1.00$, but their CCN activity is difficult to assess by the approach in this
600 study. Because the main component of these non-hygroscopic particles is estimated to be
601 elemental carbon [*Kuwata et al*., 2006], they are probably aggregates and have non-spherical
602 shapes. Conversely, it may be reasonable to assume that more-hygroscopic particles are
603 spherical under dry conditions. This is because (1) mixtures of many different organic
604 compounds are not likely to form single non-spherical crystals, (2) even liquid ammonium
605 sulfate particles dried ($d_{mob} < 200$ nm) form nearly spherical particles [*Zelenyuk et al.*, 2006],
606 and (3) electron micrograph study of more-hygroscopic particles classified by HTDMA
607 revealed that they are spherical, not like chain agglomerates or flakes as in the case of
608 less-hygroscopic particles [*McMurry et al*., 1996]. The validity of this assumption is further
609 discussed in section 3.4.3.

610 The good agreement between the predicted and measured CCN distributions as a
611 function of *g* shows that the introduction of surface tension reduction [*Facchini et al.*, 1999]
612 is not necessary for explaining the data presented in Figure 8. Furthermore, B_{83} is nearly equal
613 to B_{ss}, which suggests that dissociation and dissolution of organics via the increase in RH
614 from 83% to supersaturation is not necessary either for explaining the measured CCN activity
615 of particles. This result might be in contrast to the fact that B_{83}/B_{ss} for pure $(NH_4)_2SO_4$ and
616 NH_4NO_3 particles whose dry diameters are 100 nm are to some extent lower than unity (0.79
617 and 0.66, respectively). This difference possibly relates to the result that the mass of these
618 inorganic salts measured by the AMS is only half of that of organics, leading to different
619 non-ideal behavior.
620 With the application of the some other CCN activation models [*Kreidenweis et al.*,
621 2005], the threshold *B* is lower than presented in Figure 8. For instance, if K2005 (see section
622 2.5) is used to determine the supersaturation in the CCN counter, the supersaturation
623 condition for the experiment shown in Figure 8 is calculated to be 0.28%. This lowers the
624 thresholds of *B* to 0.29, 0.15 and 0.044 for 80, 100 and 150 nm particles, respectively. In this
625 case, B_{83}/B_{ss} and/or $\Delta\sigma/\sigma$ need to be much larger than unity to match the predicted and
626 measured of the CCN distributions. The $\Delta\sigma/\sigma$ value larger than unity is contradictory to the
627 hypothesis that organics in aerosol particles lower the surface tension [*Facchini et al.*, 1999].
628 Moreover, it is difficult to reasonably explain B_{83}/B_{ss} being significantly larger than unity,
629 because both the dissolution/dissociation of organics by dilution, and the presence of
630 $(NH_4)_2SO_4$ and NH_4NO_3 lower the B_{83}/B_{ss} ratio from unity.
631 It is, however, difficult to conclude that KP gives a better prediction of supersaturation
632 than K2005. In the study by *Kreidenweis et al.* [2005], K2005 predicts supersaturation similar
633 to some other models, e.g., a model based on literature values of water activity and density of
634 $(NH_4)_2SO_4$ particles [*Tang and Munkelwitz*; 1994]. If we assume that K2005 gives a better

635 prediction, this suggests that our measurement and/or interpretation based on Equations 1-3
636 are systematically biased. Kinetic limitation of hygroscopic growth [*Chuang*, 2003; *Chan and*
637 *Chan*, 2005] and CCN activation [*Chuang et al.*, 1997], and gas/particle re-equilibration of
638 soluble trace gases in the CCN counter [*Laaksonen et al.*, 1998] are possible explanations, but
639 their magnitudes are unknown. Since there is so far no means for judging which model gives
640 the most accurate estimate of the supersaturation in the CCN counter, we use KP as a base
641 model in this study to avoid the introduction of B_{83}/B_{ss} and a value of $\Delta\sigma/\sigma$ significantly
642 larger than unity. Results from K2005 are also discussed to assess the potential uncertainty of
643 the discussion.
644
645 **3.4.2 Case 2: Unpredicted CCN fraction is present**
646 In contrast to the results shown in Figures 8a-c, the numbers of CCN larger than that
647 predicted by the assumptions above (i.e., application of KP to determine the supersaturation
648 RH, $\Delta\sigma/\sigma = 0$, and $B_{83}/B_{ss} = 1.0$) were observed over substantial time periods. Figure 9a is an
649 example of such cases for particles whose dry diameters are 100 nm. In this case, the
650 predicted number of CCN particles is only less than half of that measured. Although some
651 multiply charged particles classified in DMA1 [*Wiedensohler*, 1988] should be detected as
652 CCN active just because of their larger size, the fraction of the multiply charged particles was
653 minor throughout the study (16 ± 3% for 100 nm particles).
654 Temporal variation of supersaturation (random error: 5%) may in part be responsible
655 for the deviation of the threshold of B, but the magnitude may not fully explain the differences
656 in CCN distributions shown in Figures 8 and 9a. Table 3 presents a sensitivity study of
657 thresholds of B and g in the case that the set point of supersaturation is 0.22%. It is shown that
658 the possible random errors in the thresholds of B and g are mainly associated with the random
659 error in s_c, and those from other factors, RH and $d_{mob,dry}$ (which relate to the precision of g in

660 Table 2), are minor. Change in the threshold of B as a result of changes in s_c from +1 to –1 SD
661 is 20% (= +10.8%– (–9.3%)), whereas the difference in the threshold of B required to explain
662 Figures 8 and 9 are 50%, which corresponds to 5 SD change of s_c.
663 A likely explanation for the discrepancy between the measured and predicted CCN
664 distributions is that either or both of the assumptions of $\Delta\sigma/\sigma = 0$ and $B_{83}/B_{ss} = 1$ are not
665 appropriate in the case presented in Figure 9a. First, if we assume that hygroscopicity B
666 measured using HTDMA is not largely different from that under the supersaturation condition
667 ($B_{83} \approx B_{ss}$), the presence of unexpected CCN suggests that the surface tension of particles
668 could be lower than that of pure water (See possible changes of the threshold for different
669 $\Delta\sigma/\sigma$ values in Figure 9a). *Facchini et al*., [1999] has suggested based on their fog
670 measurements that surface tension reduction due to organic compounds in aerosol particles
671 could be 25% lower under supersaturation conditions. We applied the 25% decrease in the
672 surface tension, and calculated the shift in the threshold of B and g to be CCN active (Figure
673 9b). The distribution of predicted CCN as a function g is also recalculated accordingly. As
674 shown in Figure 9b, the decrease in surface tension significantly increases the predicted CCN
675 number, and the majority of the unexpected CCN fraction is explained. Some CCN fraction
676 below the threshold is still not predicted, but such a small fraction may be explained by the
677 presence of multiply charged particles and their non-spherical shapes. Since the relationship
678 between the surface tension reduction and the shift in the threshold was calculated based on a
679 constant σ value around the critical droplet diameter (see Equation 3), the relationship is
680 potentially biased if the surface tension is not constant near the critical supersaturation
681 condition. However, the difference is probably negligible as is discussed in section 3.4.4.
682 The difference in hygroscopicity B under sub- and supersaturated conditions (i.e.
683 $B_{83}/B_{SS} \neq 0$) is also possibly responsible for the unexpected CCN fraction in Figure 9a. The
684 threshold of B on the assumption that $\Delta\sigma/\sigma$ = -25% (Figure 9b) is equivalent to the change in

685 hygroscopicity explained by $B_{83}/B_{SS} = 0.42$. Such difference in the hygroscopicity B could be
686 caused by the RH dependence of the non-ideality term $\nu\phi$ and the degree of dissolution ε
687 [*Schulman et al.*, 1996]. If the particle is assumed to be composed of an insoluble core and an
688 $(NH_4)_2SO_4$ (or NH_4NO_3) solution shell, the threshold of g corresponding to 0.22%
689 supersaturation was calculated to be 1.25 (or 1.23), which fails to explain the CCN
690 distribution (see Figure 9). The B_{83}/B_{ss} ratios for $(NH_4)_2SO_4$ and NH_4NO_3 in the core-shell
691 models are 0.81 and 0.66, respectively, which are close to those for pure $(NH_4)_2SO_4$ (0.79)
692 and NH_4NO_3 (0.66). In addition, if only inorganic salts generally govern B_{83}/B_{ss} as in the
693 core-shell model, it is difficult to explain the deviation of the B thresholds between Figure 8b
694 (case 1) and Figure 9b (case 2). Moreover, the influence of inorganic salts on B_{83}/B_{ss} may be
695 limited because the fraction of sulfate and nitrate in the particles are probably rather small
696 (Figure 7 and Table 2). Hence, the organic component present in particles is more likely to be
697 responsible for the low B_{83}/B_{ss} ratio. They may also relate to the variation of the ratio, in
698 addition to that originating from Δs_c (Table 3). If the non-ideality term $\nu\phi$ of organics is
699 different from inorganic salt, and if the soluble fraction ε is less than unity for some organics,
700 the organics significantly affect the RH dependence of hygroscopicity B. In this case, change
701 in the mixing ratios of organics and inorganic salts may lead to the observed variation of
702 B_{83}/B_{ss}. Furthermore, temporal variation of characteristics of organics, e.g., the degree of
703 oxidation, may also change B_{83}/B_{ss} via changes in $\nu\phi$ and ε.

704 As explained in the previous section, application of the K2005 model to the prediction
705 of supersaturation conditions leads to a substantial increase in the predicted CCN numbers. In
706 the case of the aerosol sample shown in Figure 9, the estimated threshold of B based on
707 K2005 is 0.15, which gives a prediction similar to Figure 9b. However, as described above,
708 application of K2005 in turn overpredicts the CCN numbers in the cases in Figure 8, which is
709 difficult to explain without introducing biases that have not already been taken into account in

this study.

3.4.3 Particle morphology

It is useful to assess the potential errors of the prediction of CCN numbers if dry particles classified in DMA1 are not perfect spheres. If particles are non-spherical, the volume equivalent diameter d_{ve} is smaller than the mobility diameter d_{mob}. Given that dry particles of more-hygroscopic mode are non-spherical or porous and that they are spherical after humidification in the HTDMA, the substitution of $d_{ve,dry}$ by $d_{mob,dry}$ as in this study leads to an underestimation of hygroscopicity in sub- and supersaturated conditions. Although the errors in two different conditions in part cancel out in the comparison between g and s_c, underestimation of the hygroscopicity B and overestimation of $d_{ve,dry}$ in Equation 3, overall leads to an overestimation of the critical supersaturation s_c.

As an extreme case for more-hygroscopic particles, we assume that the dynamic shape factor χ of dry particles in DMA1 is 1.18, which is for cubic particles whose $d_{mob,dry}$ is 100 nm [*Biskos et al.*, 2006]. In the case of particles whose apparent g is 1.30 (equal to the calculated threshold of g to be CCN active in Figure 8b), $d_{ve,dry}$ is calculated to be 9% smaller than $d_{mob,dry}$, which gives errors of +10% in predicted s_c. The error of the predicted s_c is equivalent to a shift in the threshold of apparent g from 1.30 to 1.25 (see Figure 8a). Therefore, predicted CCN numbers on the assumption of a potential non-spherical shape is to some extent larger than those presented in Figure 8. However, the shift in the threshold does not fully explain the measured CCN numbers. Further, the error in the prediction of CCN numbers for ambient particles in the more-hygroscopic mode may be smaller, because their shape under dry conditions may be closer to spheres than to cubic particles. This is supported by the result that dry ammonium sulfate particles have a dynamic shape factor in free molecular regime χ_v less than 1.04 for d_{mob} <200 nm, and that addition of organics to ammonium sulfate particles

735 further lowers χ_v [*Zelenyuk et al*., 2006]. We thereby conclude that the possible nonsphericity
736 of more-hygroscopic particles may have a limited effect on the discussion here. It should be
737 noted, however, that the sensitivity of s_c to the dynamic shape factor χ is a function of g, and
738 that it is significantly high if g is very close to unity with less hygroscopic particles.
739
740 **3.4.4 Changes in surface tension and hygroscopicity in supersaturation conditions**
741 In section 3.4.2, negative $\Delta\sigma/\sigma$ values and B_{83}/B_{ss} less than unity were introduced to
742 explain the unexpected CCN fraction. The calculation was based on Equation 3; $\Delta\sigma/\sigma$ and B_{ss}
743 are assumed to be constant near the critical supersaturation condition. However, the values of
744 $\Delta\sigma/\sigma$ and B_{ss} of atmospheric particles are not necessarily constants in supersaturation
745 conditions. The errors associated with this simplification are assessed in this section.
746 As a preliminary assessment of the non-constant surface tension, we applied the
747 relationship between σ and Water Soluble Organic Carbon (WSOC) concentration presented
748 by *Facchini et al.* [1999]. In this model, as the droplet diameter increases with humidification,
749 the WSOC concentration decreases by the dilution in particle liquid water. The surface tension
750 then increases monotonically, which eventually approaches the surface tension of pure water.
751 We estimated the σ - d_{ve}(RH) relationship by assuming that WSOC is completely dissolved
752 regardless of the amount of liquid water. Surface tension reduction by insoluble organic films,
753 micelle formation [*Tabazadeh*, 2005], and the effect of surfactant partitioning to the Raoult
754 effect [*Sorjamaa et al.*, 2004] are not considered here. In the case that $\Delta\sigma/\sigma$ is fixed at –25.0%
755 near the critical supersaturation condition and that $d_{mob,dry}$ = 100 nm and Bss = B_{83} = 0.265,
756 the critical supersaturation s_c was calculated from Equation 3 to be 0.14%. Next we calculated
757 s_c numerically, applying $\Delta\sigma/\sigma$ as a function of d_{ve}(RH) [*Facchini et al.*,1999]. The WSOC
758 fraction in particles was adjusted so that the same critical supersaturation condition (0.14%)
759 was established without changing $d_{mob,dry}$, Bss and B_{83} values. In this numerical calculation,

760 $\Delta\sigma/\sigma$ under critical supersaturation conditions was calculated to be –25.4%. The difference of
761 $\Delta\sigma/\sigma$ in the two model cases (with constant and variable σ) is very small (0.4%), supporting
762 the validity of using Equation 3 with constant σ in the supersaturation condition. It should be
763 noted, however, that the error in $\Delta\sigma/\sigma$ depends on the σ - d_{ve}(RH) relationship applied, and
764 the error in $\Delta\sigma/\sigma$ under supersaturation conditions is larger or smaller if the other model
765 relationships are applied [e.g., *Li et al.*, 1998; *Sorjamaa et al.*, 2004]. Qualitatively, the error
766 of the prediction based on Equation 3 could be larger if the slope of the function $\sigma =$
767 $f(d_{ve}(\mathrm{RH}))$ near the supersaturation condition is larger.
768 Similar to the case of non-constant surface tension, if the hygroscopicity B near the
769 critical supersaturation condition is not constant, application of Equation 3 leads to the error
770 in the $s_c - B_{SS}$ relationship. The perturbation is negligible in the cases of the insoluble core -
771 $(NH_4)_2SO_4$ (or NH_4NO_3) shell model; The errors in B_{83}/B_{SS} for fixed s_c (0.22%) is less than
772 0.01. However, the magnitude of the error cannot be assessed for atmospheric particles
773 because of the lack of information about the B - d_{ve}(RH) relationship.
774
775 **3.5 Role of organics in the CCN numbers**
776 For the aerosol particles measured in this study, the CCN number concentrations at the
777 inlet of DMA2 were calculated by integrating the measured CCN number distributions as a
778 function of hygroscopic growth factor g (e.g., the red histograms in Figures 8 and 9). Further,
779 CCN concentrations are predicted based on the modeled CCN – g relationship (e.g., the blue
780 histograms in Figures 8 and 9a and the green histogram in Figure 9b). In Figure 10, measured
781 and predicted CCN number concentrations are plotted for all the samples when the dry
782 particle diameters were 100 nm and the supersaturation condition was 0.22%. Here results
783 from both KP and K2005 are presented for comparison. In each figure, the predicted CCN
784 number concentrations are plotted for three different cases; the reduction of surface tension

785 $\Delta\sigma/\sigma$ is 0, -12.5, and -25% whereas B_{83}/B_{SS}=1. They are equivalent to the assumptions that
786 B_{83}/B_{SS} are 0.42, 0.67 and 1 in the case $\Delta\sigma/\sigma$=0. In Figure 10a (KP), most of the data points
787 for the assumptions $\Delta\sigma/\sigma$ = 0 and B_{83}/B_{SS}=1 are between the 1:1 and 1:2 lines, indicating that
788 this base case predicts about 50-100% of the CCN present, depending on the time period. The
789 average of the ratios of predicted for the measured CCN numbers ($N_{CCN,pred}/ N_{CCN,meas}$) in the
790 base case is 0.59 (1SD: 0.24). Few data points are above the 1:1 line, suggesting that any
791 mechanism to reduce the CCN activity relative to the base model ($\Delta\sigma/\sigma$ = 0 and B_{83}/B_{SS}=1) is
792 unnecessary. The predicted CCN on the assumption that $\Delta\sigma/\sigma$ = -25% (or B_{83}/B_{SS} = 0.42) are
793 between the 1:1 and 2:1 lines. In this case, the average of $N_{CCN,pred}/ N_{CCN,meas}$ is 1.68 (one
794 standard deviation: 0.57).
795 In the case of K2005 (Figure 10b), CCN numbers are overpredicted for many of the
796 samples. In the base case ($\Delta\sigma/\sigma$ = 0, B_{83}/B_{SS} = 1), many of the data points are between the 1:1
797 and 2:1 lines. The reduction of surface tension ($\Delta\sigma/\sigma$ < 0), and dissolution/dissociation by the
798 dilution (B_{83}/B_{SS} < 1) further enhance the discrepancy between the predicted and measured
799 CCN numbers. As explained above, the $N_{CCN,pred}/ N_{CCN,meas}$ ratio higher than unity for the base
800 case ($\Delta\sigma/\sigma$ = 0, B_{83}/B_{SS} = 1) is less realistic than that less than unity, and hence suggests
801 systematic errors in the measurement/analysis and/or K2005. In any case, the
802 sample-to-sample deviation of the $N_{CCN,pred}/ N_{CCN,meas}$ ratios in the base case is similar for both
803 KP and K2005.
804 Based on the difference between measured and predicted CCN number concentrations,
805 we calculated the possible reduction of surface tension in the case that B_{83}/B_{SS} = 1. Figure 11
806 plots the frequency distribution of samples as a function of $\Delta\sigma/\sigma$. Here only the result from
807 KP is presented. Our data suggests that the surface tension reductions were in the range of
808 –25%-+10% during the sampling period. The mode values of the frequency were from –15%
809 to -10%, and 76% of samples (29 among 38) were from –20% to -5%. Additionally, the

B_{83}/B_{SS} ratio, in the case that reduction of surface tension is negligible, is presented in the top axes. The difference in B_{83}/B_{SS} is up to two fold, and the relative standard deviation is 19%. This deviation is about a factor of two larger than that estimated from random errors in the measurement (see Table 3).

Although there may be room for discussion on the uncertainty of the supersaturation conditions in the CCN counter, the results in Figures 10 and 11 are in agreement with the hypothesis that characteristics originating from organic compounds in particles influence the CCN activity of atmospheric particles. It should be noted that water-soluble organics also contribute to the CCN activity via the solute effect [*Dick et al*., 2000], and contributions of water-soluble organics might be important even in the case of Figure 8. Our HTDMA-CCNC experiment suggests that, in addition to the solute effect of water-soluble organics, other factors associated with organics could also affect the CCN activity of urban aerosol particles.

3.6 Chemical compositions and the CCN activity

As discussed above, comparison between predicted and measured CCN numbers strongly depend on the models used to predict supersaturation in the CCN counter, which limits the interpretation of the data. On the other hand, the deviation of $N_{CCN,pred}/ N_{CCN,meas}$ from its average is not sensitive to the applied model (KP or K2005). Here we present a preliminary assessment of the relationship between $N_{CCN,pred}/ N_{CCN,meas}$ and chemical compositions of more-hygroscopic mode particles estimated from the AMS data. Chemical components other than EC in Table 2 are assumed to be entirely present in more-hygroscopic mode particles. It should be noted that this assumption is not necessarily true because some fraction may have been associated with less-hygroscopic particles, although heating at 400 °C in VTDMA did not lead to significant change in the d_{mob} of less-hygroscopic particles [*Kuwata et al.*, 2006]. In this analysis, organic components are subdivided into

hydrocarbon-like organics and oxygenated organics according to the analytical procedure of the AMS data in *Zhang et al.* [2005b].

Table 4 presents correlations of $N_{CCN,pred}/N_{CCN,meas}$ with ratios of different chemical components. All of the correlations presented in Table 4 are statistically significant. In particular, the correlation between $N_{CCN,pred}/N_{CCN,meas}$ and the ratio of the hydrocarbon-like organic mass (HOM) (or oxygenated organic mass (OOM)) to the total organic mass (OM) was substantial, implying a relationship between CCN activity and the characteristics of the organic compounds. The presence of correlations between $N_{CCN,pred}/N_{CCN,meas}$ and chemical composition supports the interpretation that the observed variation of the $N_{CCN,pred}/N_{CCN,meas}$ ratio is not merely random noise caused by fluctuations of s_c and other variables.

The correlation between HOM/OM (or OOM/OM) and $N_{CCN,pred}/N_{CCN,meas}$ indicates that the underprediction of the CCN numbers are significant for samples whose HOM/OM is relatively large. Although the correlation does not necessarily mean that the fraction of hydrocarbon-like organics is casually associated with CCN activity, it may be worth noting that the relationship is consistent with the hypothesis of the potential effects of organics on CCN activity (sections 3.4 and 3.5). Possible explanations are that hydrocarbon-like organics are associated with surface-active organics, and/or that hydrocarbon-like organics contain slightly soluble compounds that substantially enhance partitioning in the aqueous phase under RH conditions above 83%. Because the HTDMA-CCNC and the AMS did not measure exactly the same fraction of atmospheric particles, the quantitative relationship has not been assessed in more detail in this study. More experiments are required to clarify the linkages between organic composition and CCN activity using the HTDMA-CCNC system coupled to the AMS.

3.7 Comparison with previous CCN studies and future perspectives

860 As explained in the introduction section, hygroscopicity and CCN activity of
861 atmospheric aerosol particles have been measured simultaneously in several field studies
862 [*Brechtel and Kreidenweis*, 2000a; *Zhou et al.*, 2001; *Dusek et al.*, 2003; *Roberts et al.*, 2004;
863 *Rissler et al.*, 2005]. Some studies overpredicted CCN concentrations by about 30 % [*Zhou et*
864 *al.*, 2001; *Dusek et al.*, 2003], whereas *Rissler et al*. [2004] suggested that the application of
865 the measured hygroscopicity at 90% RH using HTMDA and of the surface tension of pure
866 water to the Köhler equation well predict the measured CCN numbers within a 25% error.
867 Although our study does not give a full answer to the potential difference in measured and
868 predicted CCN numbers, results in Figures10 and 11 suggest that factors associated with
869 organics cause some deviation of the measured CCN numbers from prediction. This
870 implication is due to the high sensitivity of the CCN numbers to the factors associated with
871 organics in our HTDMA-CCNC analysis. Different from previous studies, CCN activity and
872 hygroscopicity of particles have been investigated for specific particle sizes, and CCN activity
873 has been assessed for particles with specific hygroscopicity.
874 As discussed in this paper, the non-ideality of the droplet solution, i.e., RH dependence
875 of hygroscopicity B is an important factor for the prediction of CCN activity from HTDMA
876 data. In previous studies, CCN activity has been typically estimated from the HTDMA data
877 assuming a mixture of an inorganic solution and an insoluble core. In this case, the
878 non-ideality of the solution is taken into account by applying a ϕ-RH relationship of known
879 inorganic compounds, such as $(NH_4)_2SO_4$. However, such RH dependence of ϕ (or B) is
880 basically not assumed for the prediction of CCN in this study. This is to simplify the
881 discussion, but also because non-ideality of the organic-inorganic mixture is not necessarily
882 similar to that of major inorganic salts such as $(NH_4)_2SO_4$. Activity coefficients of water in
883 many organic solutions are more than unity, whereas those for $(NH_4)_2SO_4$ are less than unity,
884 which means that even the sign of $\Delta B/\Delta RH$ between sub- and supersaturated conditions

depends on the solute compounds. Therefore, it is possible that the non-ideal behavior of ambient particles are substantially different from pure inorganic salts, in particular when the organic fraction is very large as observed in this study.

A novel approach to evaluate the relationship between hygroscopicity at sub- and supersaturated conditions and CCN activity using HTDMA data has recently been proposed by *Kreidenweis et al*. [2005]. Their approach was similar to that in this study, but they proposed to extrapolate the hygroscopicity *B* measured at subsaturation RH (up to 95%) to that at supersaturation, using a polynomial function of water activity obtained by the HTDMA. Although their approach does not clarify the degree of dissolution/dissociation that occurs above the upper limit of RH in the HTDMA, this approach is worth investigating in future studies using the HTDMA-CCNC system to improve the prediction of hygroscopicity *B* at supersaturation conditions.

This study shows that deviation in CCN activity caused by surface tension reduction ranging from $\Delta\sigma/\sigma$ = -25 % to 0% is, at least theoretically, detectable with the precision of the HTDMA-CCNC measurements. Although the HTDMA-CCNC approach does not give full information on the surface tension of particles, this approach may compensate for the weakness of the bulk surface tension measurement [*Facchini et al.*, 1999; *Facchini et al.*, 2000], where the difference in chemical characteristics between externally mixed particles is completely lost. In addition, surface tension measured in the bulk sample is not necessarily equal to that at the particle surface, because some insoluble surfactants may accumulate at the interface and the difference in surface/volume ratios between submicron particles and bulk solutions might lead to a large difference in the surface tension. In this sense, the HTDMA-CCNC measurements, which may give a lower limit to the surface tension, is a promising means for measuring the surface tension in the form of aerosol particles.

4. Summary

A newly developed HTDMA-CCNC system was deployed for the field measurement of hygroscopicity and CCN activity of urban aerosol particles in Tokyo in November 2004. The CCN activity was successfully measured for particles with specific dry diameters and hygroscopicity in externally mixed aerosols. This approach made it possible to assess the relationship between hygroscopicity and CCN activity in detail, in a novel manner that has not been conducted in previous field studies using a HTDMA and a CCN counter.

The CN and CCN spectra as a function of hygroscopic growth factor clearly showed that hygroscopicity of particles, which is regulated by their chemical composition, is a critically important factor for the CCN activity of urban aerosol particles. Furthermore, the spectra also showed that increases in the particle size and the supersaturation make less hygroscopic particles CCN active. The measured CCN distribution as a function of hygroscopicity is quantitatively evaluated based on Köhler theory, and it has been found that the predicted CCN activity – hygroscopic growth factor relationship based on the Köhler model in many cases does not fully explain the measured CCN numbers. Furthermore, variations of the ratios of the predicted to measured CCN numbers are larger than predicted from the precision of the supersaturation. Although the estimate of the supersaturation condition in the CCN counter, in terms of precision and trueness, may need further evaluation, the results are reasonably explained if factors other than the hygroscopicity of particles under subsaturated conditions are responsible for the measured CCN activity. The factors may include reduction of surface tension due to organics, dissolution/dissociation of slightly water-soluble organics, and the difference in non-ideality between organics and inorganic salts. These factors associated with organics potentially contribute to the CCN activity of urban aerosol particles.

Chemical compositions obtained by the AMS operated in parallel to HTDMA-CCNC

system gave additional information that supports our interpretation of the observed relationship between hygroscopicity and CCN activity. Temporal variations of the spectra of hygroscopicity and CCN numbers were confirmed to be in accordance with those of chemical compositions. Furthermore, a correlation between organic composition and the ratios of predicted to measured CCN numbers was found to be present. This implies that the variation of the ratios of the predicted to measured CCN numbers are not noise, and that the composition of organics is responsible for the variation.

In current cloud models, CCN activity of particles is in many cases regulated only by their size. Many field, laboratory and modeling studies are being conducted to assess the importance of the chemical compositions of particles for cloud processes. Our study demonstrates that the HTDMA-CCNC system deployed for field experiments is a promising tool for assessing the importance of chemical characteristics. Future studies using the HTMDA-CCNC system may contribute to extending our knowledge of the relationship among chemical composition, hygroscopicity and CCN activity of atmospheric aerosol particles.

Acknowledgements This study is in part supported by the Ministry of Education, Science, Sports, and Culture through Grants-in-Aid 14204055 and 14658149.

954 **References**

955 Abdul-Razzak, H. and S. J. Ghan. (2004), Parameterization of the influence of organic
956 surfactants on aerosol activation, *J. Geophys. Res. 109*, D03205,
957 doi:10.1029/2003JD004043.
958 Biskos, G., L. M. Russell, P. R. Buseck, and S. T. Martin (2006), Nanosize effect on the
959 hygroscopic growth factor of aerosol particles, *Geophys. Res. Lett., 33*, L07801,
960 doi:10.1029/2005GL025199.
961 Brechtel, F. J., and S. M. Kreidenweis (2000a), Predicting particle critical supersaturation
962 from hygroscopic growth measurements in the humidified TDMA. Part I: Theory and
963 sensitivity studies, *J. Atmos. Sci.*, *57*, 1854-1871.
964 Brechtel, F. J., and S. M. Kreidenweis (2000b), Predicting particle critical supersaturation
965 from hygroscopic growth measurements in the humidified TDMA. Part II: Laboratory
966 and ambient studies, *J. Atmos. Sci.*, *57*, 1872-1887.
967 Chan, M. N. and C. K. Chan (2005), Mass transfer effects in hygroscopic measurements of
968 aerosol particles, *Atmos. Chem. Phys., 5*, 2703–2712.
969 Chuang, P. Y., R. J. Charlson, and J. H. Seinfeld (1997), Kinetic limitations of droplet
970 formation in clouds, *Nature, 390*, 594-596.
971 Chuang, P. Y. (2003), Measurement of the timescale of hygroscopic growth for atmospheric
972 aerosols, *J. Geophys. Res.*, 108(D9), 4282, doi:10.1029/2002JD002757.
973 DeCarlo, P. F., J. G. Slowik, D. R. Worsnop, P. Davidovits, and J. L. Jimenez (2004), Particle
974 morphology and density characterization by combined mobility and aerodynamic
975 diameter measurements. Part 1: Theory, *Aerosol Sci. Technol., 38*, 1185-1205.
976 Dick, W. D., P. Saxena, and P. H. McMurry (2000), Estimation of water uptake by organic
977 compounds in submicrion aerosols measured during the Southeastern Aerosol and
978 Visibility Study, *J. Geophys. Res., 105*, 1471-1479.
979 Dusek, U., D. S. Covert, A. Wiedensohler, C. Neusüss, D. Weise, and W. Cantrell (2003),
980 Cloud condensation nuclei spectra derived from size distributions and hygroscopic
981 properties of the aerosol in coastal south-west Portugal during ACE-2, *Tellus*, *55B*, 35-53.
982 Facchini, M. C., M. Mircea, S. Fuzzi, and R. J. Charlson (1999), Cloud albedo enhancement
983 by surface-active organic solutes in growing droplets, *Nature, 401*, 257-259.
984 Facchini, M. C., S. Decesari, M. Mircea, S. Fuzzi, and G. Loglio (2000), Surface tension of
985 atmospheric wet aerosol and cloud/fog droplets in relation to their organic carbon content
986 and chemical composition, *Atmos. Environ., 34*, 4853-4857.
987 Feingold, G. and P. Y. Chuang (2002), Analysis of the influence of film-forming compounds

on droplet growth: Implications for cloud microphysical processes and climate, *J. Atmos. Sci., 59*, 2006-2018.

Gasparini, R., R. Li, and D. R. Collins (2004), Integration of size distributions and size-resolved hygroscopicity measured during the Houston Supersite for compositional categorization of the aerosol, *Atmos. Environ., 38*, 3285-3303.

Ghan, S., N. Laulainen, R. Easter, R. Wagener, S. Nemesure, E. Chapman, Y. Zhang, and R. Leung (2001a), Evaluation of aerosol direct radiative forcing in MIRAGE, *J. Geophys. Res. 106*, 5295-5316.

Ghan, S., R. Easter, J. Hudson and F.-M. Bréon (2001b), Evaluation of aerosol indirect radiative forcing in MIRAGE, *J. Geophys. Res., 106*, 5317-5334.

Hämeri, K., M. Väkevä, H.-C. Hansson, and A. Laaksonen (2000), Hygroscopic growth of ultrafine ammonium sulfate aerosol measured using an ultrafine tandem differential mobility analyzer, *J. Geophys. Res*., *105*, 22,231-22,242.

Hänel, G., 1976: The properties of atmospheric aerosol particles as functions of the relative humidity at thermodynamic equilibrium with the surrounding moist air. *Adv. Geophys., 17*, 73–188.

Heintzenberg, J., A. Maßling, and W. Birmili (2001), The connection between hygroscopic and optical particle properties in the atmospheric aerosol, *Geophys. Res. Lett., 28*, 3649-3651.

Jayne, J. T., D. C. Leard, X. Zhang, P. Davidovits, K. A. Smith, C. E. Kolb, and D. R. Worsnop (2000), Development of an aerosol mass spectrometer for size and composition analysis of submicron particles, *Aerosol Sci. Technol., 33*, 49-70.

Kreidenweis, S. M., K. Koehler, P. J. DeMott, A. J. Prenni, C. Carrico, and B. Ervens (2005), Water activity and activation diameters from hygroscopicity data – Part I: Theory and application to inorganic salts, *Atmos. Chem. Phys. 5*, 1357-1370.

Köhler, H. (1936), The nucleus in and the growth of hygroscopic droplets, *Trans. Faraday Soc.*, *32*, 1152-1161.

Kuwata, M. et al. (2006), paper in preparation.

Laaksonen, A., P. Korhonen, M. Kulmala, and R. J. Charlson (1998), Modification of the Kohler equation to include soluble trace gases and slightly soluble substances, *J. Atmos. Sci., 55*, 853-862.

Lance, S., A. Nenes, and T. A. Rissman (2004), Chemical and dynamical effects on cloud droplet number: Implications for estimates of the aerosol indirect effect, *J. Geophys. Res., 109*, D22208, doi:10.1029/2004JD004596.

1022 Li, Z., A. L. Williams, and M. J. Rood (1998), Influence of soluble surfactant properties on
1023 the activation of aerosol particles containing inorganic solute, *J. Atmos. Sci., 55*,
1024 1859-1866.
1025 Matsumoto, K., H. Tanaka, I. Nagao, and Y. Ishizaka (1997), Contribution of particulate
1026 sulfate and organic carbon to cloud condensation nuclei in the marine atmosphere,
1027 *Geophys. Res. Lett., 24*, 655-658.
1028 McMurry, P. H., M. Litchy, P.-H. Huang, X. Cai, B. J. Turpin, W. D. Dick, and A. Hanson
1029 (1996), Elemental composition and morphology of individual particles separated by size
1030 and hygroscopicity with the TDMA, *Atmos. Environ., 30*, 101-108.
1031 Mochida, M. and K. Kawamura (2004), Hygroscopic properties of levoglucosan and related
1032 organic compounds characteristic to biomass burning aerosol particles, *J. Geophys. Res.,*
1033 *109,* D21202, doi:10.1029/2004JD004962.
1034 Novakov T., and J. E. Penner (1993), Large contribution of organic aerosols to
1035 cloud-condensation-nuclei concentrations *Nature, 365*, 823-826.
1036 Nenes, A., R. J. Charlson, M. C. Facchini, M. Kulmara, A. Laaksonen, and S. H. Seinfeld
1037 (2002), Can chemical effects on cloud droplet number rival the first indirect effect?
1038 *Geophys. Res. Lett., 29*, doi:10.1029/2002GL015295.
1039 O'Dowd, C. D., M. C. Facchini, F. Cavalli, D. Ceburnis, M. Mircea, S. Decesari, S. Fuzzi, Y.
1040 J. Yoon, and J.-P. Putaud, Biogenically driven organic contribution to marine aerosol,
1041 *Nature, 431*, 676-679.
1042 Pitzer, K. S., and G. Mayorga (1973), Thermodynamics of electrolytes. II. Activity and
1043 osmotic coefficients for strong electrolytes with one or both ions univalent. *J. Phys.*
1044 *Chem., 77*, 2300-2308.
1045 Pruppacher, H. R. and J. D. Klett (1997), Microphysics of clouds and precipitation, Kluwer
1046 Academic Publishers, Dordrecht, 954 pp.
1047 Raymond, T. M. and S. N. Pandis (2003), Cloud activation of single-component organic
1048 aerosol particles, *J. Geophys. Res., 107(D24),* 4787, doi:10.1029/2002JD002159, 2002.
1049 Rissler, J., E. Swietlicki, J. Zhou, G. Roberts, M. O. Andreae, L. V. Gatti, and P. Artaxo (2004),
1050 Physical properties of the sub-micrometer aerosol over the Amazon rain forest during the
1051 wet-to-dry season transition – comparison of modeled and measured CCN concentrations,
1052 *Atmos. Chem. Phys., 4*, 2119-2143.
1053 Roberts G. C., P. Artaxo, J. Zhou, E. Swietlicki, and M. O. Andreae, Sensitivity of CCN
1054 spectra on chemical and physical properties of aerosol: A case study from the Amazon
1055 Basin (2002), *J. Geophys. Res., 107(D20),* 8070, doi:10.1029/2002JD000583.

1056 Roberts, G. C. and A. Nenes (2005), A continuous-flow streamwise thermal-gradient CCN
1057 chamber for atmospheric measurements, *Aerosol Sci. Technol., 39*, 206-221.
1058 Saxena, P., L. M. Hildemann, P. H. McMurry, and J. H. Seinfeld (1995), Organics alter
1059 hygroscopic behavior of atmospheric particles, *J. Geophys. Res., 100*, 18,755-18,770.
1060 Shulman, M. L., M. C. Jacobson, R. J. Carlson, R. E. Synovec, and T. E. Young (1996),
1061 Dissolution behavior and surface tension effects of organic compounds in nucleating
1062 cloud droplets, *Geophys. Res. Lett., 23*, 277-280.
1063 Sorjamaa, R., B. Svenningsson, T. Raatikainen, S. Henning, M. Bilde, and A. Laaksonen
1064 (2004), The role of surfactants in Köhler theory reconsidered, *Atmos. Chem. Phys., 4*,
1065 2107-2117.
1066 Takegawa, N., Y. Miyazaki, Y. Kondo, Y. Komazaki, T. Miyakawa, J. L. Jimenez, J. T. Jayne,
1067 D. R. Worsnop, J. D. Allan, and R. J. Weber (2005), Characterization of an Aerodyne
1068 Aerosol Mass Spectrometer (AMS): Intercomparison with other aerosol instruments,
1069 *Aerosol Sci. Technol., 39*, 760-770.
1070 Takegawa, N., T. Miyakawa, Y. Kondo, J. L. Jimenez, D. R. Worsnop, and M. Fukuda,
1071 Seasonal and diurnal variations of submicron organic aerosol in Tokyo observed using the
1072 Aerodyne Aerosol Mass Spectrometer (2006), *J. Geophys. Res., in press*.
1073 Tang, I. N., and H. R. Munkelwitz (1994), Water activities, densities, and refractive indices of
1074 aqueous sulfates and sodium nitrate droplets of atmospheric importance, *J. Geophys. Res.,*
1075 *99*, 18,801-18,808.
1076 Tabazadeh, A. (2005), Organic aggregate formation in aerosols and its impact on the
1077 physicochemical properties of atmospheric particles, *Atmos. Environ., 39*, 5472-5480.
1078 Wiedensohler, A. (1988), Technical note: An approximation of the bipolar charge distribution
1079 for particles in the submicron range, *J. Aero. Sci., 19*, 387-389.
1080 Zelenyuk, A., Y. Cai, and D. Imre (2006), From agglomerates of spheres to irregularly shaped
1081 particles: Determination of dynamic shape factors from measurements of mobility and
1082 vacuum aerodynamic diameters, *Aero. Sci. Technol., 40*, 197-217.
1083 Zhang, Q., D. R. Worsnop, M. R. Canagaratna, and J. L. Jimenez (2005a), Hydrocarbon-like
1084 and oxygenated organic aerosols in Pittsburgh: insights into sources and processes of
1085 organic aerosols, *Atmos. Chem. Phys., 5*, 3289-3311.
1086 Zhang, Q., M. R. Alfarra, D. R. Worsnop, J. D. Allan, H. Coe, M. R. Canagaratna, and J. L.
1087 Jimenez (2005b), Deconvolution and quantification of hydrocarbon-like and oxygenated
1088 organic aerosols based on aerosol mass spectrometry. *Environ. Sci. Technol., 39*,
1089 4938-4952.

1090 Zhang, Q., M. R. Canagaratna, J. T. Jayne, D. R. Worsnop, and J. L. Jimenez (2005c), Time-
1091 and size-resolved chemical composition of submicron particles in Pittsburgh:
1092 Implications for aerosol sources and processes, *J. Geophys. Res. 110,* D07S09,
1093 doi:10.1029/2004JD004649.
1094 Zhou, J., E. Swietlicki, O. H. Berg, P. P. Aalto, K. Hämeri, E. D. Nilsson, and C. Leck (2001),
1095 Hygroscopic properties of aerosol particles over the central Arctic Ocean during summer,
1096 *J. Geophys. Res. 106,* 32,111-32,123.
1097 Xu, Q., M. DeWitte, and J. J. Sloan (2003), The effect of formic acid on the deliquescence of
1098 model sea-salt aerosol particles, *Atmos. Environ., 37*, 911-919.
1099

1099

1100 **Figure Captions**

1101

1102 **Figure 1.** Diagram of the experimental setup. The CCN counter was connected to the
1103 HTDMA in parallel to the CN counter. The AMS was operated in parallel to the HTDMA.
1104 The third DMA (DMA3) and the CN counter connected with the 400°C heater (volatility
1105 TDMA) were for quantifying non-volatile components [*Kuwata et al*., 2005]. Key: SG, Silica
1106 Gel; MS, Molecular Sieve; SMPS, Scanning Mobility Particle Sizer; DMA, Differential
1107 Mobility Analizer; CN, Condensation Nuclei; CCN, Cloud Condensation Nuclei; CPC,
1108 Condensation Particle Counter.

1109

1110 **Figure 2.** (a) An example of the measured distributions of CN (white histogram) and CCN
1111 (shaded histogram) as a function of hygroscopic growth factor *g*. (b) The ranges of the
1112 hygroscopic growth factor of the particles when CCN numbers were measured at the four
1113 fixed set points of hygroscopic growth factors (1.00, 1.11, 1.24 and 1.38). (c) Weighting
1114 functions to calculate CCN distributions.

1115

1116 **Figure 3.** Normalized distribution of hygroscopic growth factor *g* at 83% RH for 100 nm
1117 particles during the study. Mean distributions (thick solid line) and the ranges within one
1118 standard deviation (shaded area) are presented.

1119

1120 **Figure 4.** Size distributions of CN and CCN for (a) 0.22%, (b) 0.55%, (c) 0.82%, and (d)
1121 1.3% supersaturations. Size distributions averaged from 23:00, 11/14 to 21:00, 11/15 in 2004
1122 are presented. CCN distributions were determined from CCN/CN ratios measured for 30, 50,
1123 80, 100, 150, and 200 nm particles and their interpolation. In the case of (a) 0.22%
1124 supersaturation, the CCN/CN ratio was extrapolated toward larger diameters on the
1125 assumptoin that the CCN/CN ratio is unity for 300 nm particles.

1126

1127 **Figure 5.** The CCN/CN ratios measured for hygroscopic growth factors of 1.00, 1.11, 1.24,
1128 and 1.38. The hygroscopic growth factors were measured at (a-f) 83% and (g and h) 89% RH
1129 in the HTDMA, respectively. The initial dry diameters of particles were (a) 30, (b and g) 50,
1130 (c) 80, (d and h) 100, (e) 150 and (f) 200 nm. Supersaturation conditions in the CCN counter
1131 were 0.22% (open circles), 0.55% (solid triangles), 0.82% (open squares), and 1.3% (solid
1132 diamonds).

Figure 6. Temporal variations of the number distributions of (a) CN, (b) CCN at 0.22% supersaturation, and (c) CCN at 0.55% supersaturation as a function of hygroscopic growth factor *g*. Particle numbers are for sample aerosols entering DMA2. (d) Mass concentrations of inorganics and organics measured using the AMS (d_{va}: 50 - 200 nm).

Figure 7. Temporal variations of the normalized distributions of (a) CN, (b) CCN at 0.22% supersaturation, and (c) CCN at 0.55% supersaturation as a function of hygroscopic growth factor *g*. (d) Relative abundances of inorganics and organics measured using the AMS (d_{va}: 50 - 200 nm).

Figure 8. Distributions of CN (black) and CCN (red) numbers as a function of hygroscopic growth factor *g* (or hygroscopicity *B*) for the sample on November 14, 2004. The initial dry diameters were (a) 80 nm, (b) 100 nm, and (c) 150 nm. Predicted CCN distributions by assuming $\Delta\sigma/\sigma = 0\%$ have been superimposed as blue histograms. Error bars on the predicted distributions represent the random errors, which is mainly associated with the precision of s_c (see section 3.4.2 and Table 3). The vertical solid lines are the lower limits (thresholds) of *g* and *B* to be CCN at 0.22% supersaturation. The systematic errors of the thresholds are shown as vertical dotted lines. Hygroscopicity *B*, and the possible change in the threshold by that of surface tension are shown as extra *x*-axes on the figures. Supersaturation was calculated based on the KP model [*Köhler*, 1936; *Pitzer and Mayorga*, 1973]. Results based on K2005 [*Kreidenweis et al.*, 2005] are not shown here but discussed in the text. See section 2.5 for details of the KP and K2005 models.

Figure 9. Distributions of CN (black) and CCN (red) numbers as a function of hygroscopic growth factor for 100 nm particles for the sample on November 10, 2004. Predicted CCN distributions by assuming (a) $\Delta\sigma/\sigma = 0\%$ and (b) $\Delta\sigma/\sigma = -25\%$ were superimposed as (a) blue and (b) green histograms, respectively. Error bars on the predicted distributions represent the random errors. The vertical thick and dotted lines are the lower limits (thresholds) of hygroscopicity *B* (and hygroscopic growth factor *g*) to be CCN at 0.22% supersaturation and the range of the systematic error, respectively. Hygroscopicity *B*, and the possible change of the threshold by that of surface tension are shown as extra *x*-axes on the figures. Supersaturation was calculated based on the KP model. Results based on K2005 are not shown but discussed in the text.

Figure 10. Plots of predicted versus measured CCN concentrations on the assumptions that B_{83}/B_{ss}=1 and reductions of surface tension, $\Delta\sigma/\sigma$, are 0% (open blue squares), -12.5% (solid green circles), and –25% (solid red squares). Results from two different predictions of supersaturation conditions based on (a) the KP [*Köhler*, 1936; *Pitzer and Mayorga*, 1973] and (b) the K2005 [*Kreidenweis et al.*, 2005] models are presented. These plots also correspond to the case where $\Delta\sigma/\sigma$ = 0% and B_{83}/B_{ss} are 1.0 (open blue squares), 0.67 (solid green circles), and 0.42. The 1:2, 1:1 and 2:1 lines are also presented in the figure. The CCN concentrations are for sample aerosols entering DMA2 of the HTDMA system. All the multiply charged particles are assumed to be CCN active, and omitted from both measured and predicted CCN numbers. Error bars represent the systematic errors, which are associated with the trueness of the RH measurement (≤ 2%) in DMA2. The magnitude of the random errors in the predicted CCN numbers (not shown) is similar to the range of the systematic errors presented.

Figure 11. Frequency distribution of 100 nm-particle samples as a function of $\Delta\sigma/\sigma$, on the assumption that B_{83}/B_{ss}=1. The B_{83}/B_{ss} value is also shown at the top of the graph on the assumption that $\Delta\sigma/\sigma$ = 0. This figure is based on the calculation of supersaturation using the KP model. The value of $\Delta\sigma/\sigma$ (B_{83}/B_{ss}=1) corresponding to $N_{CCN\_pred}/N_{CCN\_meas}$ = 1 for each sample was obtained by linear interpolation of the relationship between $N_{CCN\_pred}/N_{CCN\_meas}$ and $\Delta\sigma/\sigma$ at $\Delta\sigma/\sigma$ =0%, -12.5% and –25% (see Figure 10). The systematic error averaged for all samples is calculated from the trueness of the RH measurement in DMA2, and is presented in the top-left of the figure. Note that B_{83}/B_{ss} of pure $(NH_4)_2SO_4$ is 0.79.

Table 1. Random and systematic errors and width of the variables in the HTDMA-CCNC experiment

Variables	Random error [a] (Precision)	Systematic error (Trueness)	Width [a]
Measured Variables			
CN count	1–4% [b]	n/a	n/a
CCN count	2–10% [b]	n/a	n/a
d_{mob} classified by DMA1	1%	Calibrated with DMA2	4%
d_{mob} classified by DMA2	1%	Used as a reference DMA, calibrated using PSL particles	4%
Supersaturation	5% [c]	Defined based on the measurement of s_c of $(NH_4)_2SO_4$ particles classified by the DMA that is calibrated with DMA2 [d]	6–11% (2–9%) [e]
RH in DMA2	0.3% (0.9%) [f]	< 2% [g]	
Derived Variables			
CCN/CN ratio	2–11%	< 10 % (Estimated based on the cases of CCN/CN ~ 1.)	n/a
Hygroscopic growth factor g	1% [h]	≤ 2% (Confirmed by the hygroscopic growth measurement of $(NH_4)_2SO_4$ at 83% RH)	5% (see Fig. 2b)

[a] One standard deviation (1SD). [b] For measurements of particles whose number concentrations ranged from 0.7 to 10 particle cm^{-3}, with an integration time of 3 min. [c] Estimated based on the variability in the three week interval. [d] From the Köhler theory combined with the Pitzer model (KP). Application of other CCN activation models is discussed in the results and discussion section. [e] Values depend on the supersaturation conditions. The widths of supersaturations including (excluding) the width of $d_{mob,dry}$ of $(NH_4)_2SO_4$ particles classified by the DMA are presented without (with) parenthesis. [f] As a result of the PID control of the humidified and dry air flows supplied to the Nafion tubes that control the RH of aerosol and sheath flows [*Mochida and Kawamura*, 2004]. Standard deviation of the RH reading at the inlet (outlet) of the DMA is presented without (with) parenthesis. [g] Manufacturer's warrant based on the calibration using Vaisala HMK15. The outlet RH equals to the inlet RH +0.2% on average. [h] Determined from growth factor measurements for 100 nm $(NH_4)_2SO_4$ particles at 83% RH.

1200

1201

1202

1203 **Table 2. Chemical compositions of aerosol particles**

1204 **(wt%) measured by AMS (d_{va}: 50–200 nm).**

component	range	mean
NO_3^-	2–23	7
SO_4^{2-}	<1–16	5
Cl^-	<1–6	2
NH_4^+	2–20	10
Organics	36–65	54
EC [a]	8–35	24

1205 [a] Since AMS does not detect elemental carbon (EC), concentrations of EC were
1206 estimated from the characteristic peak of the hydrocarbons at m/z 57, which
1207 usually correlates to the amount of EC in an urban environment [*Zhang et al.,*
1208 2005c]. The scaling factor was determined by comparison with EC
1209 concentrations obtained by a Sunset Laboratory OC/EC analyzer.

Table 3. Sensitivity analysis of the thresholds of *B* and *g* to be CCN active, in the case that the set point of the supersaturation in the CCN counter is 0.22%.

Perturbation (%) [a]	$\Delta B_{threshold}$ (%)	$\Delta g_{threshold}$ (%)
Δs_c = -5 / +5	+10.8 / -9.3	+1.9 / -1.7
ΔRH_{HTDMA} = -0.3 / +0.3 (-0.9 / +0.9 [c])	n/a [b]	+0.3 / -0.3 (+0.9 / -0.9) [c]
$\Delta d_{mob,dry}$ = -1 / +1	+3.1 / -2.9	+ 0.5 / -0.5

[a] Based on precisions in Table 1. [b] Not calculated because the perturbation of RH alters the relationship between *B* and *g* (i.e., the axes of *B* in Figure 8 and 9). [c] Based on the RH reading at the outlet of DMA2.

1220

1221

1222 **Table 4. Correlations of fractions of organics with $N_{CCN\_pred}/N_{CCN\_meas}$ [a].**

ratios [b]	r [c]	$P(r = 0)$ (%) [d]
OM/(WSIM+OM)	-0.37	4.0
HOM/(WSIM+OM)	-0.57	0.08
OOM/ (WSIM+OM)	0.47	0.7
HOM/OM	-0.63	0.02
OOM/OM	0.63	0.01

1223 [a] Number of samples is 31. The $N_{CCN\_pred}/N_{CCN\_meas}$ value is derived with
1224 the KP model. [b] OM: organic mass; WSIM: water soluble inorganic mass;
1225 HOM: hydrocarbon-like organic mass; OOM: oxygenated organic mass.
1226 Details of the determination of HOM and OOM from the AMS data are
1227 presented in *Zhang et al.* [2005b]. [c] Correlation coefficient. The errors in r
1228 associated with systematic errors in $N_{CCN\_pred}/N_{CCN\_meas}$ (see Figure 10a)
1229 are up to 0.05. [d] Limit of the probability that the null hypothesis $r = 0$ is
1230 rejected.

Fig. 1 Mochida et al.

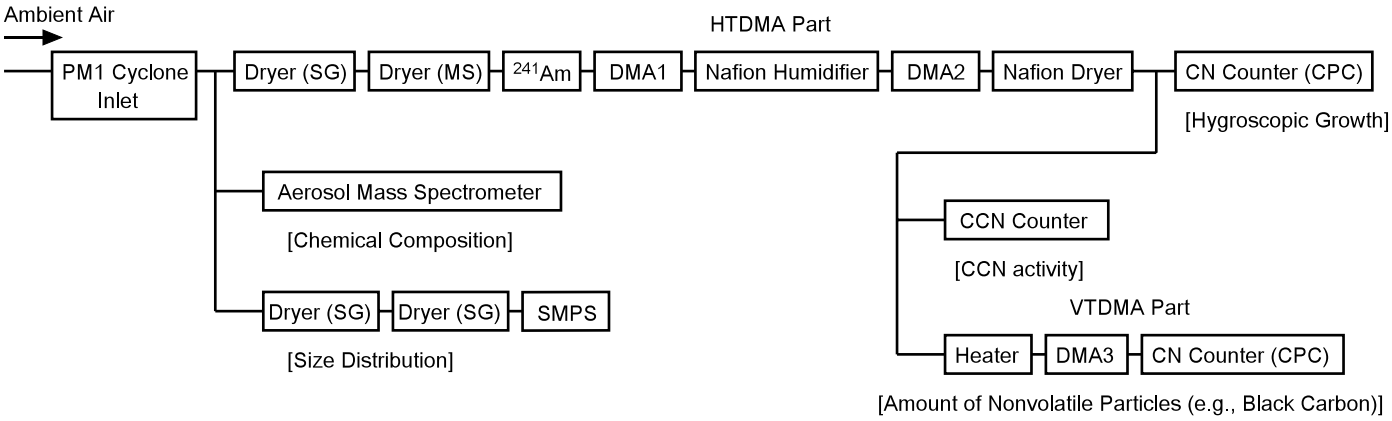

Fig.2 Mochida et al.

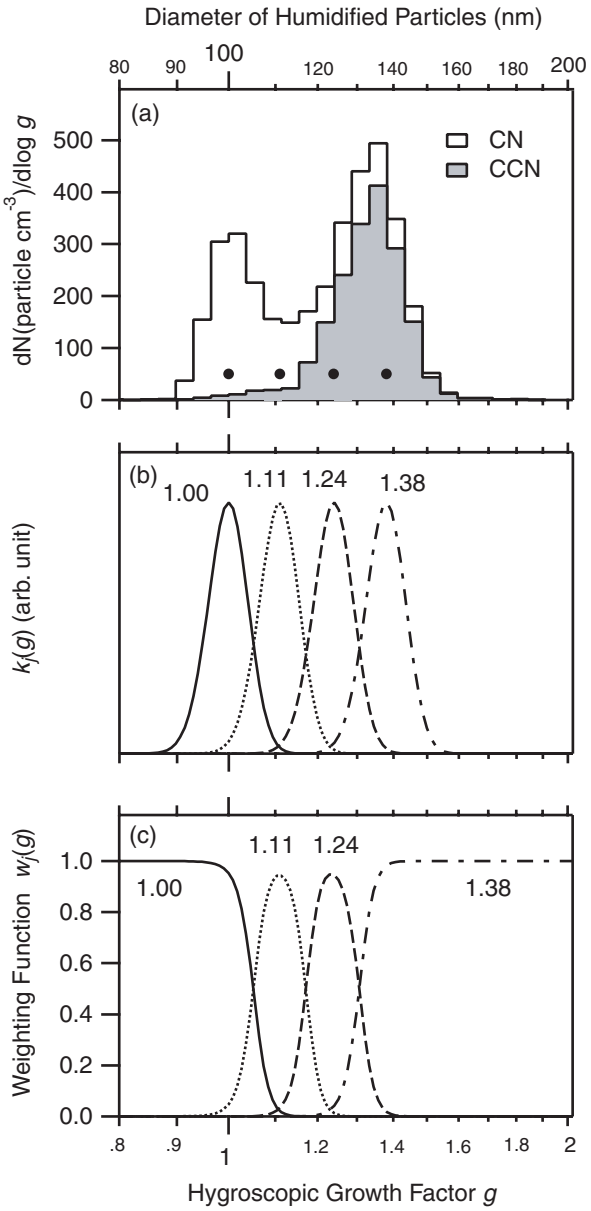

Fig. 3 Mochida et al.

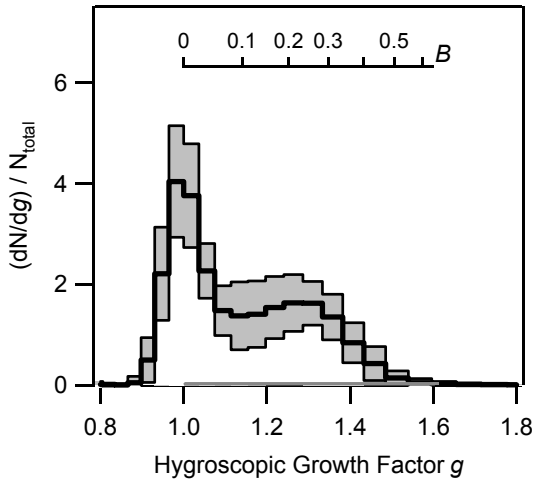

Fig. 4 Mochida et al.

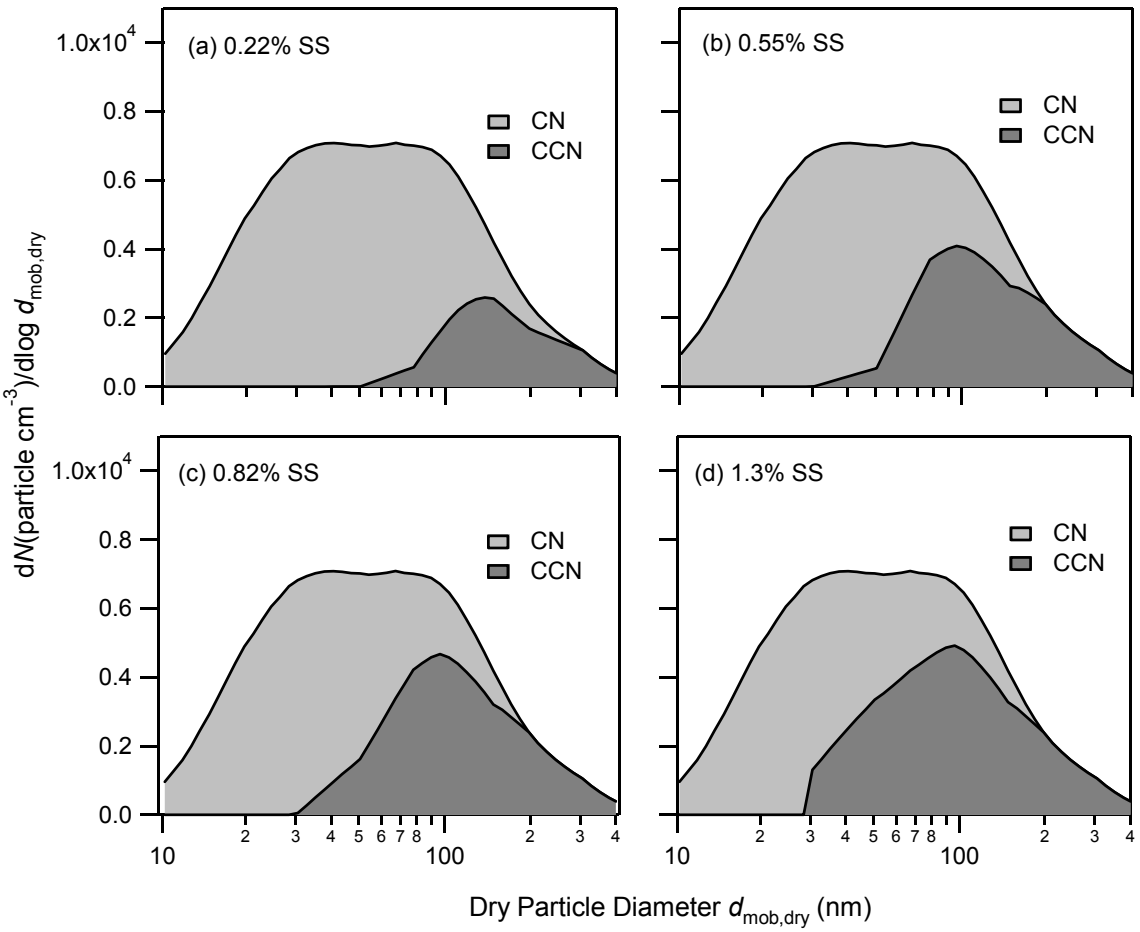

Fig. 5 Mochida et al.

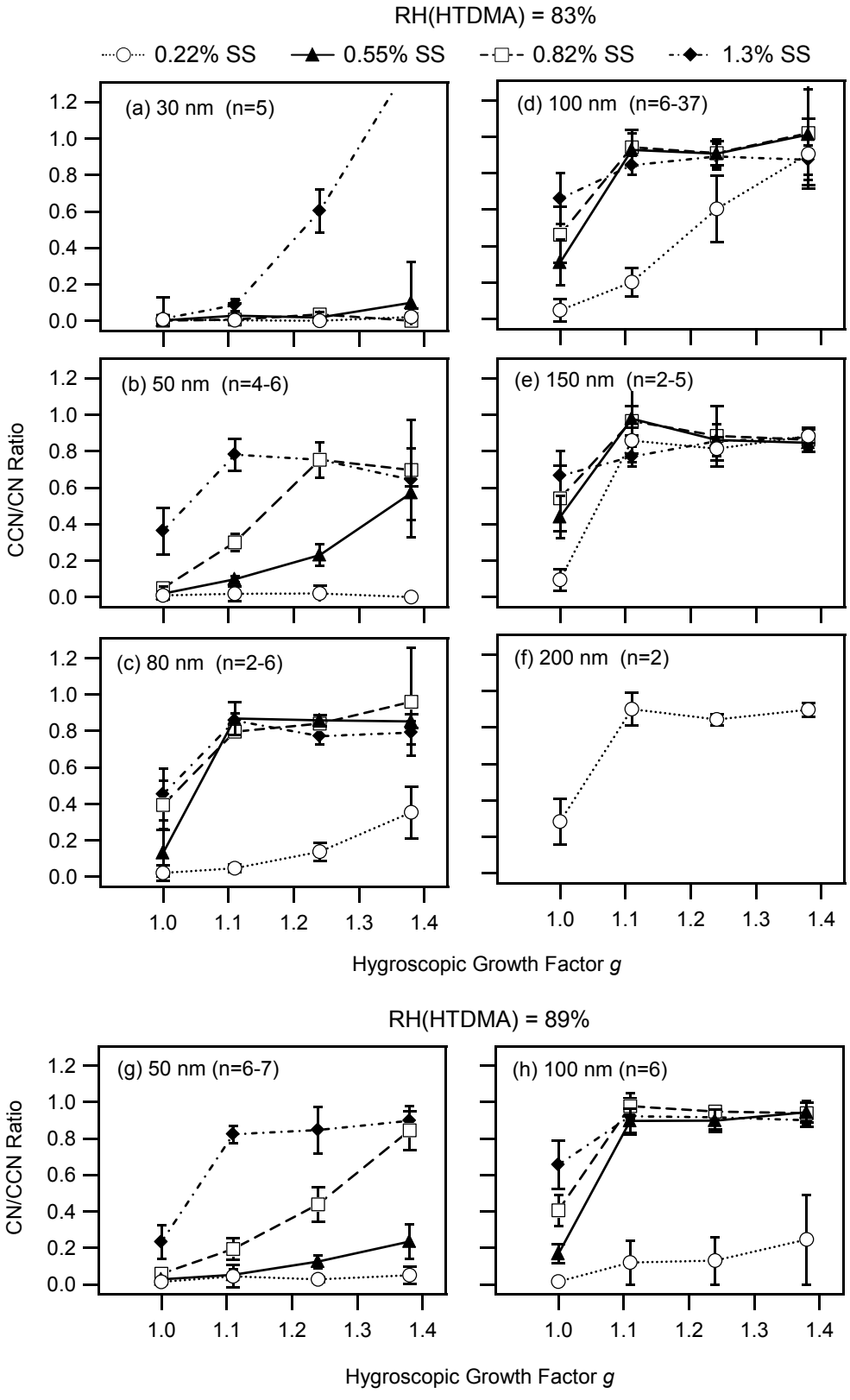

Fig.6 Mochida et al.

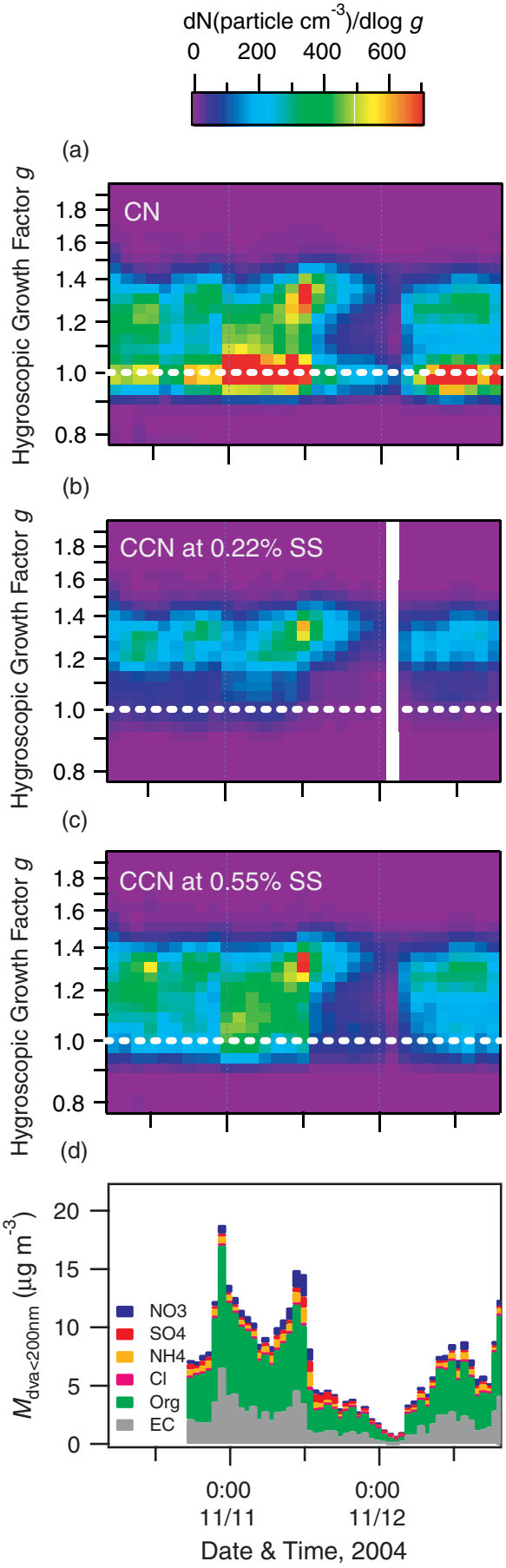

Fig.7 Mochida et al.

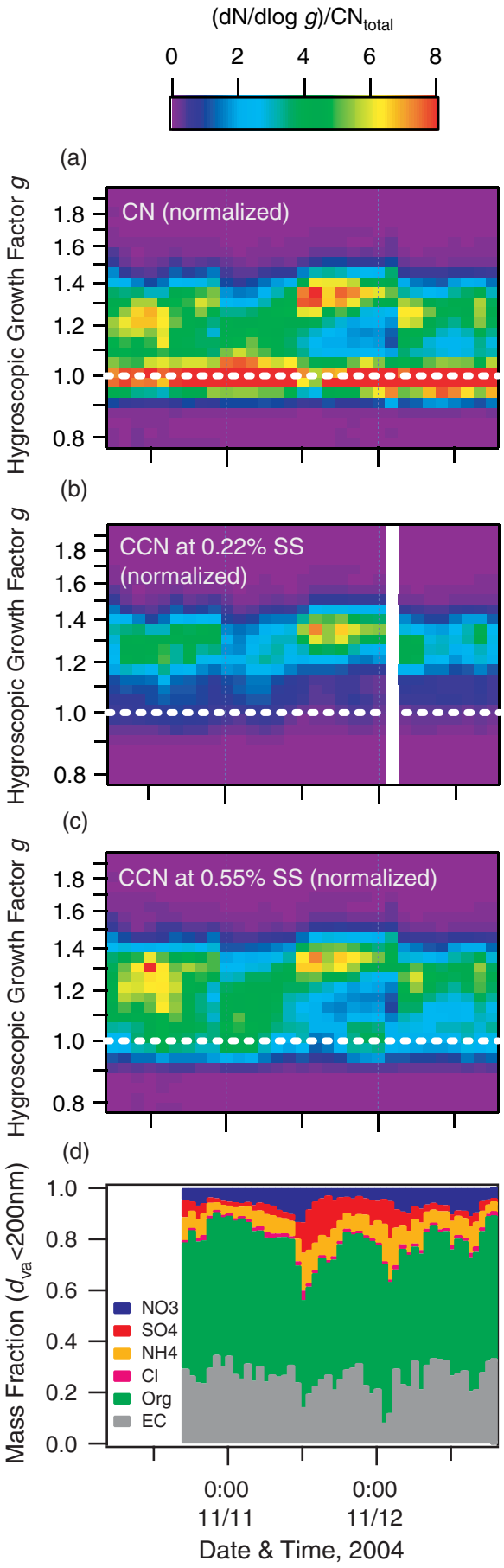

Fig. 8 Mochida et al.

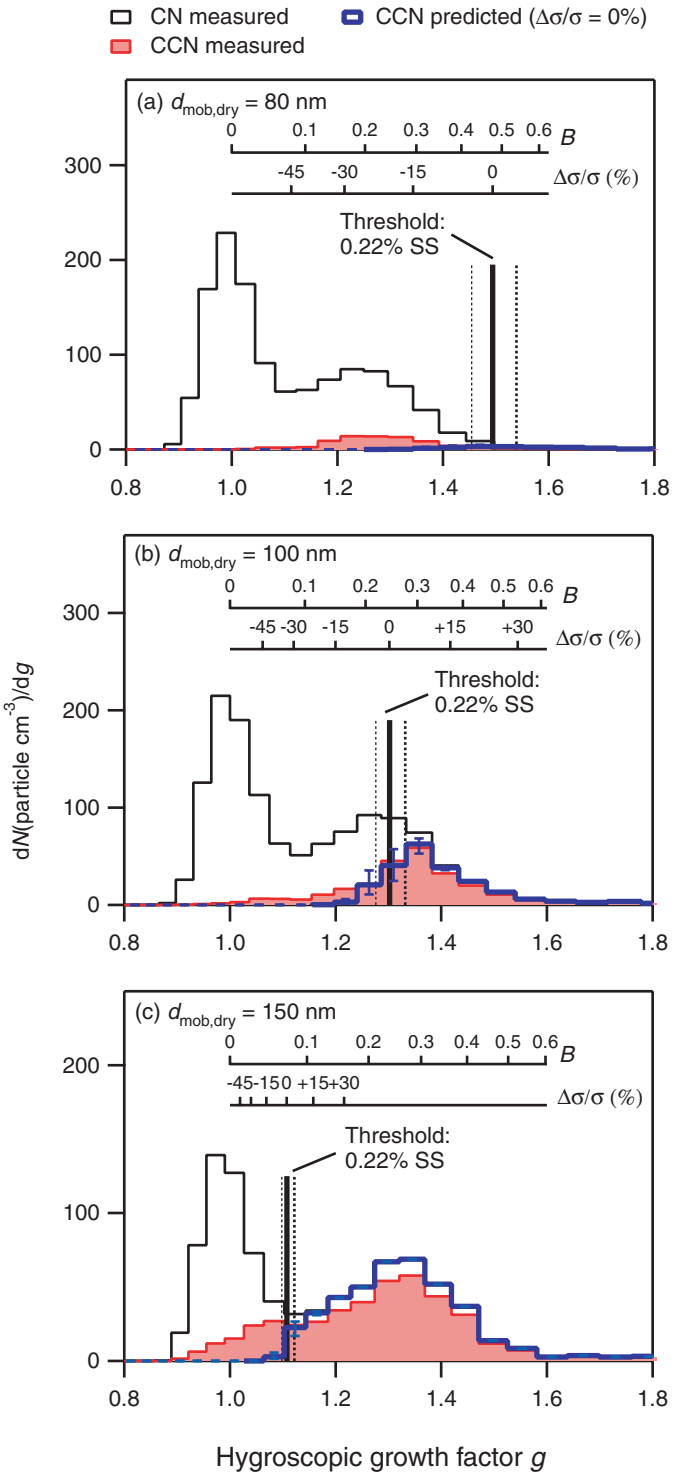

Fig. 9 Mochida et al.

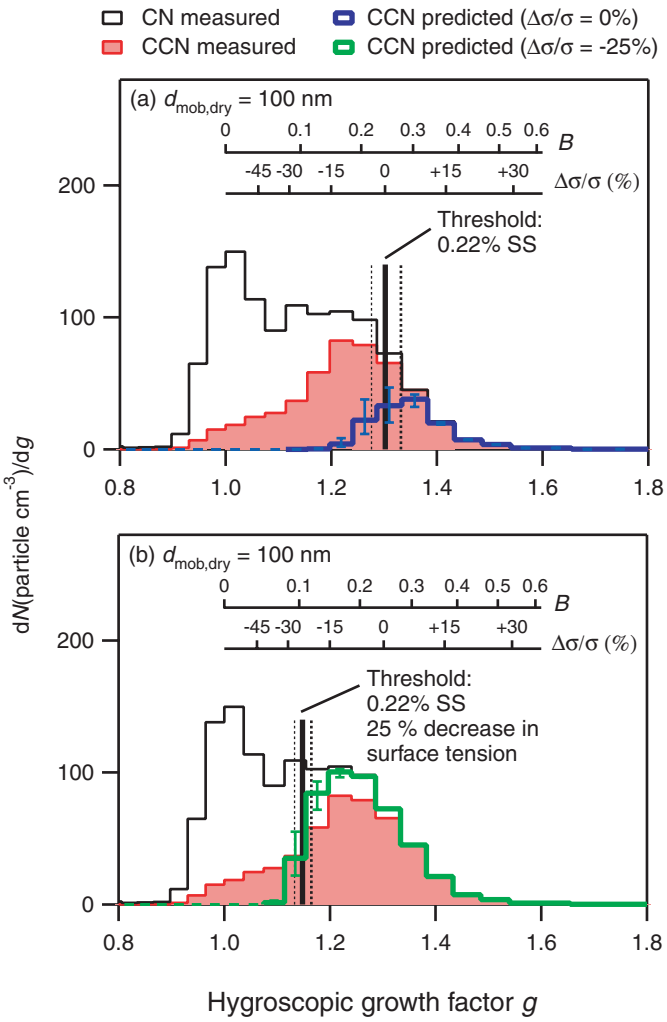

Fig. 10 Mochida et al.

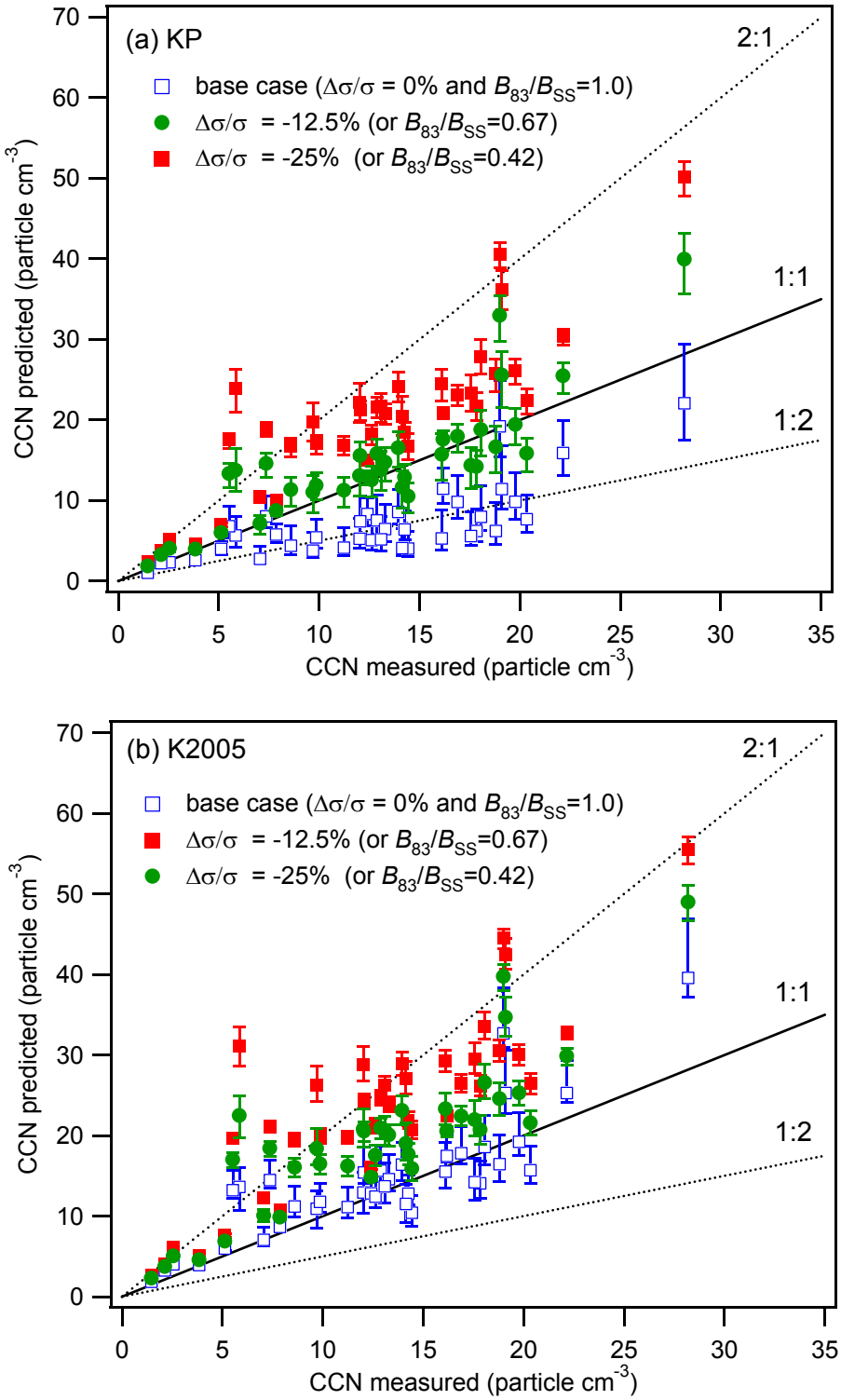

Fig. 11 Mochida et al.